Article

Cell

Long-Term Expansion of Functional Mouse and Human Hepatocytes as 3D Organoids

Graphical Abstract

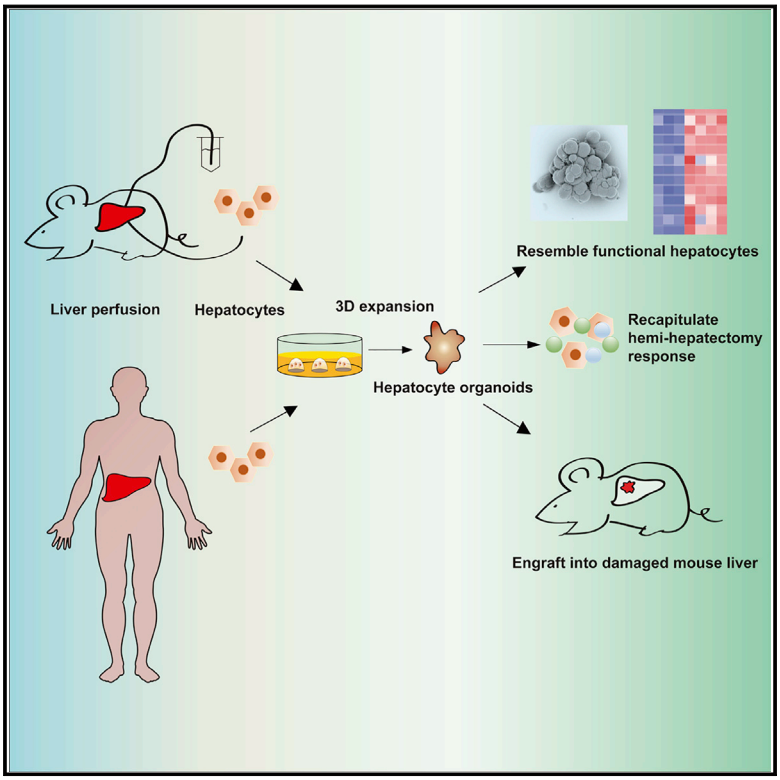

Authors

Huili Hu, Helmuth Gehart, Benedetta Artegiani, ..., Peter J. Peters, Ype P. de Jong, Hans Clevers

Correspondence

h.clevers@hubrecht.eu

In Brief

Modeling the regenerative ability of the liver in response to acute damage using long-term 3D organoid cultures in mice and human cells yields proliferative hepatocytes that are able to successfully engraft in animal models.

Highlights

- Human and mouse hepatocytes can be grown long-term as organoids
- Hepatocyte organoids consist of progenitors and differentiated hepatocytes
- Murine hepatocyte organoids reflect regeneration after partial hepatectomy
- Organoids from primary human hepatocytes engraft into damaged mouse liver

Hu et al., 2018, Cell *175*, 1591–1606
November 29, 2018
https://doi.org/10.1016/j.cell.2018.11.013

CellPress

Article

Cell

Long-Term Expansion of Functional Mouse and Human Hepatocytes as 3D Organoids

Huili Hu,[1,2] Helmuth Gehart,[1,11] Benedetta Artegiani,[1,11] Carmen LÖpez-Iglesias,[5] Florijn Dekkers,[1] Onur Basak,[1] Johan van Es,[1] Susana M. Chuva de Sousa Lopes,[6] Harry Begthel,[1] Jeroen Korving,[1] Maaike van den Born,[1] Chenhui Zou,[8,9] Corrine Quirk,[9] Luis Chiriboga,[10] Charles M. Rice,[9] Stephanie Ma,[7] Anne Rios,[4] Peter J. Peters,[5] Ype P. de Jong,[8,9] and Hans Clevers[1,3,4,12,*]

[1]Oncode Institute, Hubrecht Institute, KNAW (Royal Netherlands Academy of Arts and Sciences), Utrecht, the Netherlands
[2]The Key Laboratory of Experimental Teratology, Ministry of Education and Department of Genetics, School of Basic Medical Sciences, Shandong University, 250012 Jinan, China
[3]University Medical Center Utrecht, Cancer Genomics Netherlands, 3584CX Utrecht, the Netherlands
[4]The Princess Maxima Center for Pediatric Oncology, Utrecht, the Netherlands
[5]The Maastricht Multimodal Molecular Imaging Institute, Maastricht University, 6229 ER Maastricht, the Netherlands
[6]Anatomy and Embryology, Leiden University Medical Center, Einthovenweg, 2333 ZC Leiden, the Netherlands
[7]School of Biomedical Sciences, Li Ka Shing Faculty of Medicine, the University of Hong Kong, Hong Kong
[8]Division of Gastroenterology and Hepatology, Weill Cornell Medicine, New York, NY10065, USA
[9]Laboratory of Virology and Infectious Disease, the Rockefeller University, New York, NY 10065, USA
[10]Department of Pathology, NYU Medical Center, New York, NY10003, USA
[11]These authors contributed equally
[12]Lead Contact
*Correspondence: h.clevers@hubrecht.eu
https://doi.org/10.1016/j.cell.2018.11.013

SUMMARY

The mammalian liver possesses a remarkable regenerative ability. Two modes of damage response have been described: (1) The "oval cell" response emanates from the biliary tree when all hepatocytes are affected by chronic liver disease. (2) A massive, proliferative response of mature hepatocytes occurs upon acute liver damage such as partial hepatectomy (PHx). While the oval cell response has been captured *in vitro* by growing organoids from cholangiocytes, the hepatocyte proliferative response has not been recapitulated in culture. Here, we describe the establishment of a long-term 3D organoid culture system for mouse and human primary hepatocytes. Organoids can be established from single hepatocytes and grown for multiple months, while retaining key morphological, functional and gene expression features. Transcriptional profiles of the organoids resemble those of proliferating hepatocytes after PHx. Human hepatocyte organoids proliferate extensively after engraftment into mice and thus recapitulate the proliferative damage-response of hepatocytes.

INTRODUCTION

The liver displays a remarkable regenerative capacity in terms of recovery of mass and function upon surgical removal of up to 2/3 of its size partial hepatectomy (PHx), or after liver-wide chemical or infectious injury (Stanger, 2015). The response to partial removal of the liver is particularly impressive as it involves massive cell cycle entry of remaining mature hepatocytes without an apparent de-differentiation into a progenitor/stem cell-like state (Miyajima et al., 2014). The liver will thus grow back to its original size within 2 weeks after damage (Michalopoulos, 2010). There is good evidence for direct, slow hepatocyte expansion under steady-state conditions *in vivo*. An Axin2 lineage tracing allele demonstrates that mature hepatocytes located around the pericentral vein (PC) drive homeostatic hepatocyte self-renewal (Wang et al., 2015). Similarly, genetic lineage tracing approaches have demonstrated that periportal hepatocytes can replenish liver mass upon damage (Font-Burgada et al., 2015).

An alternative mechanism of liver repair comes into play when noxious agents (toxins, viruses) chronically affect all hepatocytes. Under these circumstances, small cells near the bile duct tree become proliferative ("oval cells"). The prevailing school of thought states that the cholangiocyte-like oval cells represent activated liver stem cells, capable of regenerating hepatocytes as well as new cholangiocytes (Evarts et al., 1987). Indeed, oval cells or atypical ductal cells expressing Epcam or Sox9 have long been regarded as bi-potential facultative stem/progenitor cells (Dollé et al., 2015; Furuyama et al., 2011; Huch and Clevers, 2011; Huch et al., 2013). While the hepatocyte-driven regenerative response dominates most types of liver repair (Grompe, 2014), the *in vivo* relevance of the oval cell response as well as its cell-of-origin have remained controversial. Indeed, several recent lineage tracing approaches failed to find support for a stem cell with cholangiocyte characteristics (Schaub et al., 2014; Yanger et al., 2014). Forbes and colleagues very recently provided definitive proof for an *in vivo* oval cell response, by cleverly obstructing hepatocyte proliferation (Raven et al., 2017). Lineage tracing revealed the cell-of-origin to not be a professional stem cell, but rather a cholangiocyte.

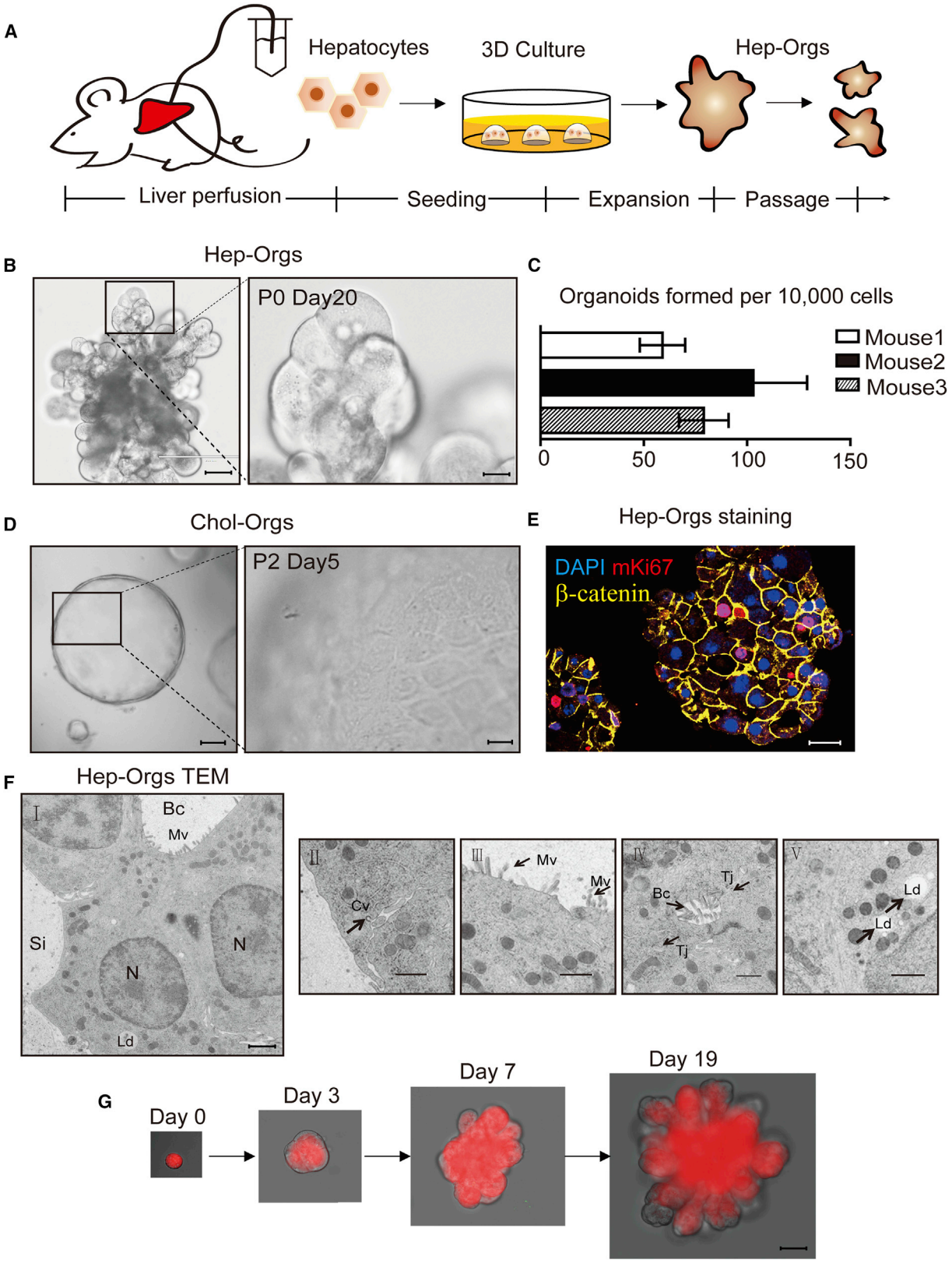

(legend on next page)

We have recently described a long-term 3D liver expansion system of mouse and human adult biliary epithelial-derived progenitor cells that mirrors the *in vivo* oval cell response (Huch et al., 2013; Huch et al., 2015). Under these defined 3D organoid culture conditions, up to a third of mature Epcam+ biliary cells are capable to undergo rapid dedifferentiation into bipotent progenitor cells that expand as cystic structures and can be passaged for over 6 months (Huch et al., 2015; Li et al., 2017). Upon removal of growth stimuli (R-spondin and forskolin), the cells regain a biliary fate. However, when Notch signaling is blocked and upon addition of FGF19, BMP7, and dexamethasone, the cells are fated toward a hepatocyte phenotype. The same protocol can be used to establish organoids of various liver cancer types (Broutier et al., 2017).

Adult mature hepatocytes can be reprogrammed into proliferative bipotent progenitor cells in response to chronic liver injury (Tanimizu et al., 2014; Tarlow et al., 2014; Yimlamai et al., 2014; Yanger et al., 2013). Indeed, mature hepatocytes have been demonstrated to display plasticity *in vivo* by transdifferentiating into cholangiocytes/biliary epithelial cells (Sekiya and Suzuki, 2014; Tanimizu et al., 2014; Yanger et al., 2014; Yanger et al., 2013). Lineage tracing has underscored the existence of hepatocyte-derived progenitor cells (hepPD); yet attempts to culture these in 3D culture initially failed (Malato et al., 2011; Tarlow et al., 2014). A recent study has described a cocktail of three small molecules that can convert rat and mouse hepatocytes *in vitro* into small, proliferative bipotent cells, termed ''chemically induced liver progenitors'' (CLiPs) in 2D. In long-term culture, CLiPs do not resemble hepatocytes morphologically, yet they retain their proliferative capacity and their hepatic differentiation ability and can repopulate a chronically injured liver (Katsuda et al., 2017).

Here we probe the direct proliferative ability of mature murine hepatocytes and human hepatocytes and describe a long-term culture system for proliferative hepatocyte organoids (Hep-Orgs), distinct from cholangiocyte derived organoids (Chol-Orgs).

RESULTS

Murine Hep-Orgs Originating from Single Mature Hepatocytes

We isolated primary hepatocytes from wild-type adult C57BL/6 mouse liver by two-step collagenase perfusion and suspended the cells in Matrigel (Figure 1A). A variety of small molecules and biologicals, including Wnt agonists such as R-spondin1 and CHIR99021; EGF, FGF7 and FGF10; HGF and the TGF-β inhibitor A83-01, were tested for the ability to support growth, (Figure S1A). During the first week of culture, small organoids emerged from Matrigel-embedded hepatocytes in some of the culture conditions. This allowed us to refine conditions, eventually resulting in robust organoid growth (Figures S1A and S1B) in the optimized Hep-Medium (Table S1). Unlike Chol-Orgs, Hep-Orgs were compact with a typical ''bunch-of-grapes'' appearance (Figure 1B in comparison to Figure 1D: Table S1 gives an overview of all comparisons). Plating efficiency was about 0.5%–1.0% of mature hepatocytes (Figure 1C). This contrasted with the high plating efficiency of biliary epithelial cells (up to 30% of purified cholangiocytes) (Huch et al., 2015; Li et al., 2017), but was similar to that of organoids derived from stomach, colon, or prostate (Bartfeld et al., 2015; Drost et al., 2016; Sato et al., 2011). The organoids expanded to a diameter of ~400 μm within 15–20 days and could be passaged by mechanical disruption at a ratio of 1:3 every 7–10 days (Video S1). Growth speed tended to slow down after 2–3 months (Figure S1C). Organoids could also be obtained from BALB/c and C57BL/6 x BALB/c mice (Figure S1D).

Figure 1E gives a confocal image section stained for the adhesion junction marker β-catenin (yellow) and the proliferation marker mKi67 (red), revealing the absence of the large lumen seen in murine Chol-Orgs (Huch et al., 2013 and Figure 2B). Typical hepatocyte morphology was revealed by transmission EM (Figure 1F).

To probe the cell-of-origin, we isolated hepatocytes from *Albumin-CreERT2*; *Rosa26-LSL-tdTomato* mice. After tamoxifen induction, ~99% of albumin-secreting hepatocytes were labeled, whereas no cells of the biliary epithelium showed recombination (Figure S1E). Single, sorted tomato-labeled hepatocytes generated fully labeled organoids, implying that the Hep-Orgs arise from single mature, albumin-expressing hepatocytes (Figure 1G).

Hepatocytes in liver lobules differentially express zonation markers along the pericentral (PC)-to-periportal vein (PP) axis (Halpern et al., 2017; Burke et al., 2009; Grün et al., 2015). During homeostasis, expression of the Wnt target gene Axin2 marks hepatocytes adjacent to the PC that are the main source of homeostatic self-renewal (Wang et al., 2015). To investigate the zonal origin of Hep-Orgs, we isolated mature hepatocytes from mice carrying *Axin2-CreERT2* and *Rosa26-LSL-tdTomato* alleles 1 week after Tamoxifen induction by FACS. Axin2+ hepatocytes displayed much higher plating efficiencies than Axin2- hepatocytes (Figure S1F). Control Epcam+ cholangiocytes generated essentially no Hep-Orgs in Hep-Medium (Figure S1G). Additionally, we sorted hepatocytes of different ploidy states (2n,

Figure 1. Establishment of 3D Culture System of Murine Hepatocyte Organoids

(A) Schematic depicting the isolation and seeding of primary hepatocytes, and the expansion and passage of Hep-Orgs.

(B) Differential interference contrast (DIC) images of Hep-Orgs at Passage 0 (P0) day 20 cultured from primary hepatocytes of wild-type C57BL/6 mice. Lower magnification (left, black scale bar = 50 μm), Higher magnification (right, black scale bar = 12.5 μm).

(C) Numbers of organoids formed per 10,000 hepatocytes. Experiments were performed in triplicate and on independent C57BL/6 mice. Data are represented as mean ± SEM.

(D) Differential interference contrast (DIC) images of Chol-Orgs at Passage 2 day 3 (left, black scale bar = 50 μm); Higher magnification (right, black scale bar = 12.5 μm).

(E) Confocal image of paraffin section of a Hep-Org co-stained for proliferation marker mKi67 (Red), the adhesion junction marker β-catenin (yellow) and DAPI (blue). Scale bar = 25 μm.

(F) Transmission EM (TEM) of Hep-orgs shows typical hepatocyte structures. (G) A clonal Hep-Org grown from a single primary hepatocyte (tdTomato+) from a tamoxifen-induced *Albumin-CreERT2; Rosa 26-LSL-tdTomato* mouse. Scale bar=25μm.

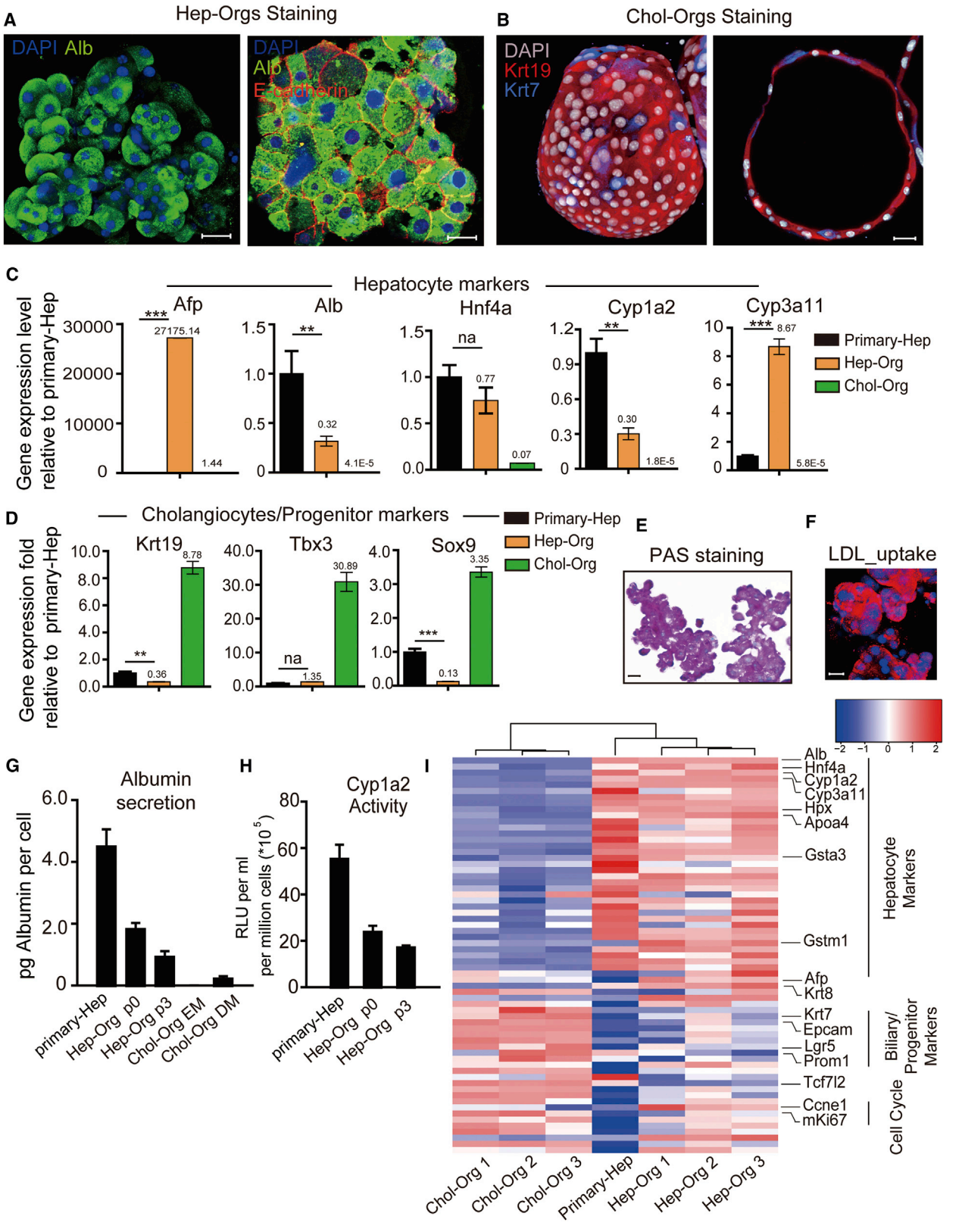

(legend on next page)

4n, and 8n) as described (Duncan et al., 2010). Tetraploid hepatocytes, common in adult mouse liver, surprisingly yielded a comparable plating efficiency to diploid cells, while octaploid cells did not grow out (Figure S1H).

Hep-Orgs Retain Key Functions and Gene Expression Profiles of Hepatocytes

Hep-Orgs were then analyzed by immunofluorescence and immuno-histochemical staining. Hep-Orgs showed strong albumin expression (green), yet were negative for the bile duct markers Krt19 or Krt7 (Figures 2A and 2B, Figures S2A and S2C). H&E, E-cadherin and β-catenin staining of paraffin sections revealed a characteristic organization of the Hep-Orgs (Figure 2A and Figure S2B). Hep-Org cells were larger in size (Figures 2A and S2B). Quantitative PCR (qPCR) was performed for the hepatocyte markers Alb, Hnf4a, Cyp1a2, and Cyp3a11, the fetal hepatocyte marker Afp, cholangiocytes/progenitor marker Krt19, and progenitor markers Tbx3 and Sox9 (Figures 2C and 2D). Expression of these markers in Hep-Orgs closely resembled that of primary mouse hepatocytes (Primary-Hep). Yet, the former re-expressed the fetal hepatocyte gene Afp, a feature of hemi-hepatectomy (Engelhardt et al., 1976; Sell et al., 1974).

Hep-Orgs showed strong periodic acid-Schiff (PAS) staining indicative of glycogen accumulation (Figure 2E). Low-density lipoprotein uptake (LDL) was readily visualized by fluorescent probes (Figure 2F). Albumin secretion of Hep-Orgs (Passage 1 (P1) and P3) was only 2- to 4-fold lower compared to primary hepatocytes. Of note, expanding Chol-Orgs secrete at least 1,000-fold less Albumin, and differentiated Chol-Orgs at least 10-fold less (Huch et al., 2013) (Figure 2G). Cytochrome activity (Cyp1a2) was also only 2- to 3-fold lower compared with primary hepatocytes (Figure 2H).

Bulk mRNA sequencing was performed for Hep-Orgs and Chol-Orgs from isolates of three different mice and compared to primary hepatocyte RNA. Figure 2I represents a heatmap of the expression for ~40 hepatocyte genes, 10 cholangiocyte/progenitor genes and a number of proliferation markers (Full gene list given in Figure S2K). Markers of hemi-hepatectomy response (Afp, cell-cycle genes) were high in Hep-Orgs, but not in primary hepatocytes. Notably, genes involved in hepatocyte functions such as Cytochrome P450 activity, glycogen metabolism, lipid metabolism, steroid metabolism, urea cycle and complement activation all displayed similar expression profiles between Hep-Orgs and primary hepatocytes (Figures S2D–S2J). Hep-Orgs expressed PC marker to a higher extent than PP markers (Figures S2L and S2M).

Hep-Orgs Recapitulate Hepatocyte Proliferation upon PHx

Gene expression patterns over time were assessed by mRNA sequencing for two murine Hep-Org cultures (M1 and M2). These remained remarkably similar over time as visualized by PCA plot and assessed at P1, P3 and P7 (Figure 3A). The heatmap of main hepatic markers such as Alb, Hnf4a, Hpx indicated their stable expression during Hep-Orgs passaging, while Krt7 and Epcam were not re-expressed (Figure 3B).

While Hep-Orgs display crucial functional aspects of primary hepatocytes, they obviously differ from these hepatocytes by being in cycle and by expressing fetal markers such as Afp (Figure 3B). PHx drives hepatocytes into proliferation, peaking at the third day after damage (Michalopoulos, 2010). To compare gene expression profiles of Hep-Orgs to the *in vivo* transcriptional state of proliferating hepatocytes, we isolated hepatocytes by collagenase digestion at day 3 post-PHx as well as control undamaged hepatocytes and performed mRNA sequencing. Hep-Orgs clustered more closely with PHx hepatocytes than with undamaged hepatocytes or Chol-Orgs (Figure 3C and Table S2). A gene set of the top-100 genes differentially expressed between PHx samples and control undamaged hepatocytes was compared to Hep-Orgs by gene set enrichment analysis (GSEA) (Table S2). Multiple genes were upregulated in proliferating hepatocytes after partial-hepatectomy that were also activated in the Hep-Orgs; gene enrichment was found in Hep-Orgs of P1, P3 and P7 (Figure 3D). In addition, we independently determined differential gene expression between PHx and control undamaged liver by microarray analysis and from this analysis we generated a gene set list including genes that changed at least 5-fold (Table S2). Significant enrichment was again observed by GSEA. Genes that were downregulated in proliferating post-PHx hepatocytes were repressed in mouse Hep-Orgs. Conversely, upregulated genes in PHx samples were enriched in Hep-Orgs (Figure 3D).

Figure 2. Characterization of Mouse Hepatocyte Organoids

(A) Confocal z stack (left) and single plane (right) images of Hep-Orgs. Albumin (green), E-cadherin (red, right panel), and DAPI (blue). Scale bar = 20 μm.

(B) Confocal z stack (left) and single plane (right) images of mouse Chol-Orgs. Krt7 (blue), Krt19 (Red), and DAPI (white). Scale bar = 20 μm.

(C and D) qRT-PCR analysis of gene expression of hepatocyte markers (C) and cholangiocyte/progenitor markers (D) in Hep-Orgs and Chol-Orgs relative to primary hepatocytes. Graph presents mean results from 4 replicates from three independent mice. Data are represented as mean ± SEM. ** indicates $p < 0.01$, *** indicates $p < 0.001$.

(E) Glycogen accumulation evaluated by Periodic-Acid Schiff (PAS) staining (dark pink) in Hep-Orgs. Nuclei were stained with hematoxylin (blue). Scale Bar = 20 μm.

(F) Low density lipoprotein (LDL) uptake was analyzed by Dil-ac-LDL fluorescent staining (Red) in cultured Hep-Orgs. Nuclei were stained with DAPI (blue). Scale bar = 20 μm.

(G) Albumin secretion measured after 24h culturing of primary hepatocytes, Hep-Orgs of Passage 0 (P0) day 15 and Passage 3 (P3) and Chol-Orgs in expansion medium (EM) or differentiation medium (DM). Results are indicated as picograms of albumin per cell. Data are represented as mean ± SEM.

(H) Measurement of cytochrome activity (Cyp1a2) in cultured primary hepatocytes, Hep-Orgs of p0 day 15 and p3. Relative light units (RLU) per ml per million cells is indicated. Data are represented as mean ± SEM.

(I) Heatmap of liver gene expression determined by mRNA sequencing comparing three independent Hep-Orgs, (p1) with primary hepatocytes (n = 1), and three independent Chol-Orgs (p8-p12) in expansion medium (EM) (full gene list in Figure S2K).

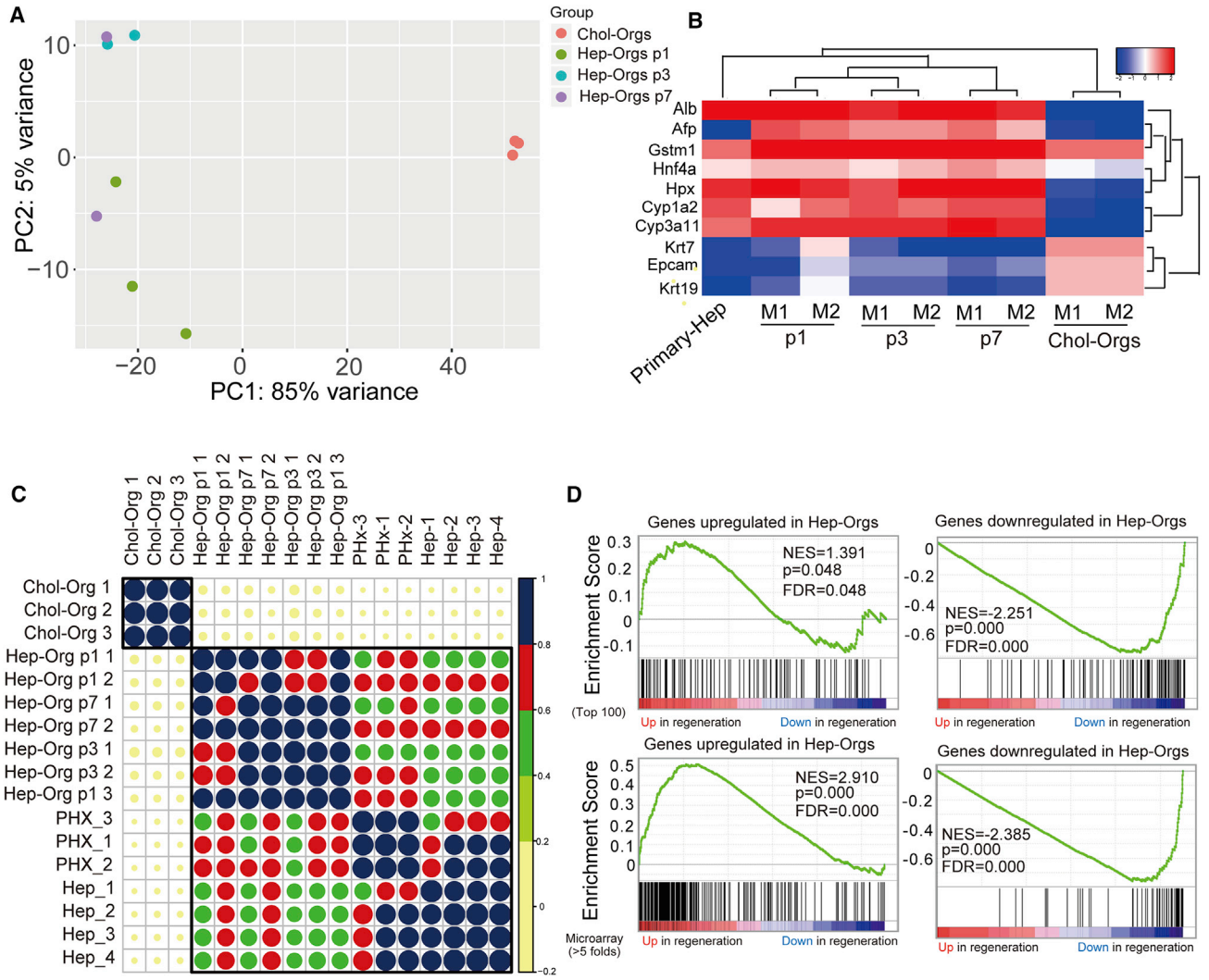

Figure 3. Hep-Orgs Recapitulate Hepatocyte Proliferation upon Partial Hepatectomy

(A) PCA plot showing the clustering of Hep-Orgs at different passages and their clear distinction from Chol-Orgs (Passage 1, 3, and 7 is labeled as P1, P3 and P7). Note the very small variance (5%) on PC2.

(B) Heatmap of major hepatic markers in primary hepatocytes, Hep-Orgs and Chol-Orgs (from M1 and M2, two separate mouse donors, Passage 1, 3, and 7 is labeled as P1, P3 and P7).

(C) Correlation plot showing Pearson's correlation coefficient between biological replicates of Chol-Orgs, Hep-Orgs at Passage 1, 3, and 7, PHx and undamaged (Hep) hepatocytes. Color intensities and the size of the circles are proportional to the correlation coefficients. Samples are ordered based on hierarchical clustering and rectangles in the graph are based on the results of the hierarchical clustering. Correlation is based on the Top 1,000-highest expressed genes (for the complete gene list see Table S2).

(D) GSEA enrichment analysis of Hep-Orgs (biological replicates at Passage 1, 3, 7) versus Primary Hepatocytes as compared to the list of differentially expressed genes between mouse liver three days post-PHx compared with non-damaged liver obtained by mRNA sequencing (top) or microarray (bottom). Enrichment of upregulated genes after 3 days of partial hepatectomy: left panel); enrichment of downregulated genes after 3 days of partial hepatectomy: right panel.

Transdifferentiation of Hep-Org Hepatocytes into Cholangiocytes

We observed that some progenitor markers like Krt8/18 and Spp1 were upregulated during liver regeneration post-PHx. An *in vivo* study has described hepatocyte-to-biliary epithelial cell conversion after injury (Yanger et al., 2013). Similarly, cholangiocarcinomas can be derived from hepatocytes upon Notch and AKT activation (Fan et al., 2012; Sekiya and Suzuki, 2014). When culturing primary hepatocytes from Albumin-CreERT2; Rosa26-LSL-tdTomato mice, cystic organoids occasionally formed when CHIR was removed. Indeed, when Tomato-positive organoids were cultured in Chol-medium for more than 10 days, Krt7/19 were strongly induced while Alb and Hnf4a expression were gradually reduced (Figures S3A and S3C). Inversely, transferring Chol-Orgs into Hep-Medium did reduce the Krt7/19 expression but did not induce expression of hepatocyte-lineage markers. (Figures S3B and S3C).

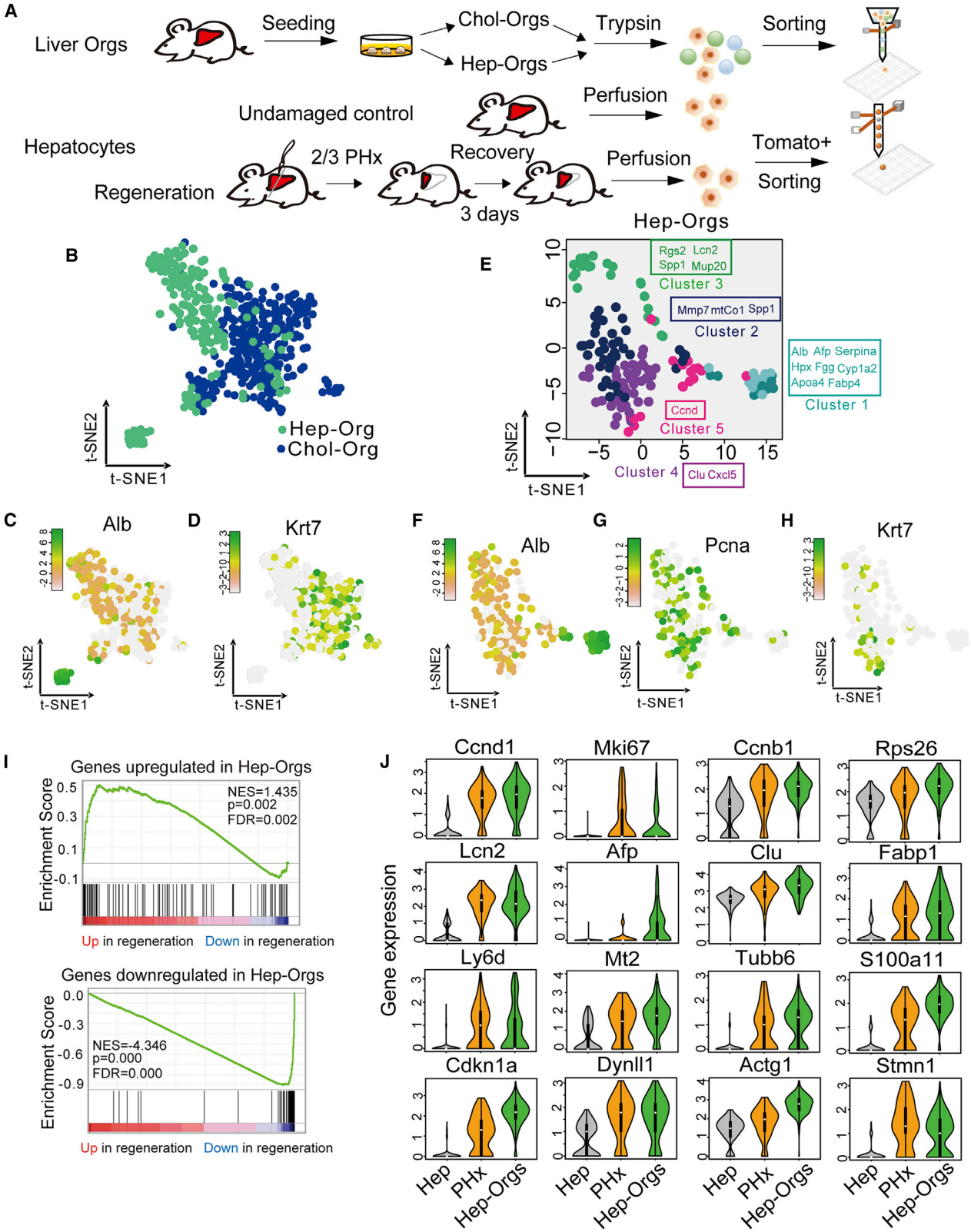

(legend on next page)

Single-Cell mRNA Analysis of Hepatocyte Organoids

Next, we performed single-cell mRNA sequencing on Hep-Orgs and Chol-Orgs (Figure 4A). We sequenced 384 cells from each and analyzed the results by RaceID2 (Grün et al., 2015). After filtering for cells with >4,000 transcripts, a total of 186 cells from Hep-Orgs and 253 cells from Chol-Orgs were retained for analysis. We performed analysis of combined datasets from Hep-Orgs and Chol-Orgs and visualized gene expression by t-SNE (Figure 4B). Consistently, Alb, Ahsg, Afp, Fgg, and Gc were only highly expressed in Hep-Orgs population while Epcam and Krt7 were highly expressed in Chol-Orgs (Figures 4C–4D, and Figures S4A and S4B). Both organoid types contained proliferating cells (Figure S4C).

We then performed a clustering analysis on cells derived only from the Hep-Orgs, to address their cellular composition (Figure 4E and Table S3). Five different clusters were identified. Cluster 1 represented non-cycling mature hepatocytes (Figures 4F and S4D shows high albumin and hepatic marker expression). Clusters 2 and 3 expressed lower levels of albumin, high levels of hepatocyte progenitor markers such as Spp1 (Liu et al., 2015) and represented cycling hepatocyte progenitor cells (Figure 4G and Figure S4E). Cluster 4 expressed high levels of cycling markers and lacked mature markers, identifying it as a yet more primitive cycling cell population. In some cells of Cluster 5, we noted expression of cholangiocyte-lineage markers such as Krt7 (Figure 4H), suggestive of a trans-differentiation event.

197 post-PHx hepatocytes and 291 undamaged hepatocytes by single-cell sequencing were also retained for analysis after filtering for >3,000 transcripts per cell. The top 100 differentially expressed genes between these were grouped in a gene set that was then used for GSEA of Hep-Orgs (Figure S4F and Table S2). Hep-Orgs were more comparable to proliferating, post-PHx hepatocytes than to control hepatocytes (Figure 4I). We used violin plots to visualize gene expression in undamaged hepatocytes, in PHx hepatocytes and in cells from Hep-Orgs. As expected, cell-cycle-related and ribosome synthesis genes were significantly increased in both Hep-Org cells and in post-PHx hepatocytes (Figure 4J). Typical non-cell-cycle-related genes that were upregulated after partial-hepatectomy showed concordant expression in Hep-Orgs. These included Afp, Lcn2, Actg1, Fabp5, Clu, Ly6d, Mt2, S100a11, Stmn1, Tubb6, Cdkn1a, and Dynll1 (Figure 4J).

Establishment and Characterization of Hep-Orgs from Human Hepatocytes

The Hep-Org medium was optimized for clonogenicity and expansion of human hepatocytes (Hep-Medium) (Figures S5A and S5B). We isolated human fetal liver cells from donor embryos of 11–20 weeks of gestation. Human fetal Hep-Orgs (Fetal-Orgs) could be established from 7 out of 8 fetal donor tissues, each displaying the typical grape-like structure (Figure 5A). Five of these could be expanded for >16 passages and were still growing exponentially at a split ratio of 1:3 every 7–10 days at the time of manuscript resubmission. The longest culture is currently at Passage 28 (fetal origin: 18 weeks post-gestation, 11 months of culture). We also established Hep-Orgs (PHH-Orgs) from cryopreserved pediatric and adult primary human hepatocytes (PHHs). These appeared to be more limited in their expansion times (2–2.5 months) yet yielded organoids of very similar composition when compared to the fetal cultures with plating efficiency of around 1% (Figures 5A and 5B). Unlike Chol-Orgs, human Hep-Orgs contained small lumina and consisted of large cells of hepatocyte morphology (Figure 5C, Figures S5C–S5E, Video S2 and Table S1). Human Hep-Orgs have a larger cell diameter than Chol-Orgs, and a lower nucleus/cytoplasm ratio (cell diameter/nucleus diameter: 30.08 ± 8.17 μm/14.07 ± 1.59 μm for Fetal-Orgs, 27.54 ± 6.50 μm/11.69 ± 1.64 μm for PHH-Orgs and 10.42 ± 2.78/7.22 ± 1.55 μm for Chol-Orgs). Transmission EM revealed an abundance of glycogen particles in the cytoplasm. Typical liver hepatocyte features included nuclei with prominent nucleoli with fibrillar centers and decondensed chromatin, large numbers of mitochondria with few and short cristae, and individual cisternae of RER organized around them. Also, Golgi apparatus saccule stacks, bile canaliculi, tight junctions, peroxisomes, lysosomes, multi-vesicular bodies and autophagic vacuoles were present in human Hep-Orgs, closely resembling those of hepatocytes (Figures 5D and 5E).

Fetal-Orgs abundantly expressed ALB and HNF4A, while a significant portion of cells expressed CYP2E1 (Figure 5F and Figure S5F). Striking networks of bile canaliculi were revealed by MRP2 staining (Figure 5G, Video S3). DiI-Ac-LDL and strong periodic acid-Schiff (PAS) staining in Fetal-Orgs indicated functional LDL uptake and confirmed glycogen accumulation (Figures 5H and 5I). Hep-Orgs did not demonstrate cholangiocyte function: Rhodamine123, a fluorescent substrate for the cholangiocyte surface glycoprotein multidrug resistance protein-1 (MDR1), was actively transported into the lumen of Chol-Orgs

Figure 4. Single-Cell Transcriptome Analysis of Hep-Orgs

(A) Overview of single-cell sequencing experiment of Hep-Orgs and Chol-Orgs and hepatocytes isolated from *Albumin-CreERT2*; *Rosa26-LSL-tdTomato* mice ("undamaged control") or 3 days after 2/3 partial hepatectomy ("regeneration").

(B) t-SNE maps indicating origin of individual cells: Hep-Org cells (green), Chol-Org cells (blue).

(C-D) t-SNE plot showing the expression of Alb (C) and Krt7 (D) in single cells derived from Hep-Orgs and Chol-Orgs. Expression is given as normalized log2 value.

(E) t-SNE map of all cell clusters from Hep-Orgs obtained by RaceID2 algorithm.

(F-H) t-SNE plot showing the expression levels of Alb (F), Pcna (G), and Krt7 (H) in Hep-Orgs. Expression is given as normalized log2 value.

(I) GSEA of genes in Hep-Orgs versus primary hepatocytes. Expression enrichment was compared to a gene set of differentially expressed genes generated by comparing mouse liver three days after partial hepatectomy compared with control non-damaged liver. Enrichment of upregulated genes at 3 days post-PHx: upper panel; enrichment of downregulated genes at 3 days of post-PHx (lower panel).

(J) Violin plot comparing the expression of markers in undamaged hepatocytes, post-PHx hepatocytes isolated and Hep-Orgs. Expression of cell-cycle-/growth-related genes is given in the top row. Markers were selected for their specific expression in regenerating liver, but unrelated to cell cycling (bottom-three rows). Transcript counts are provided on log10 scale.

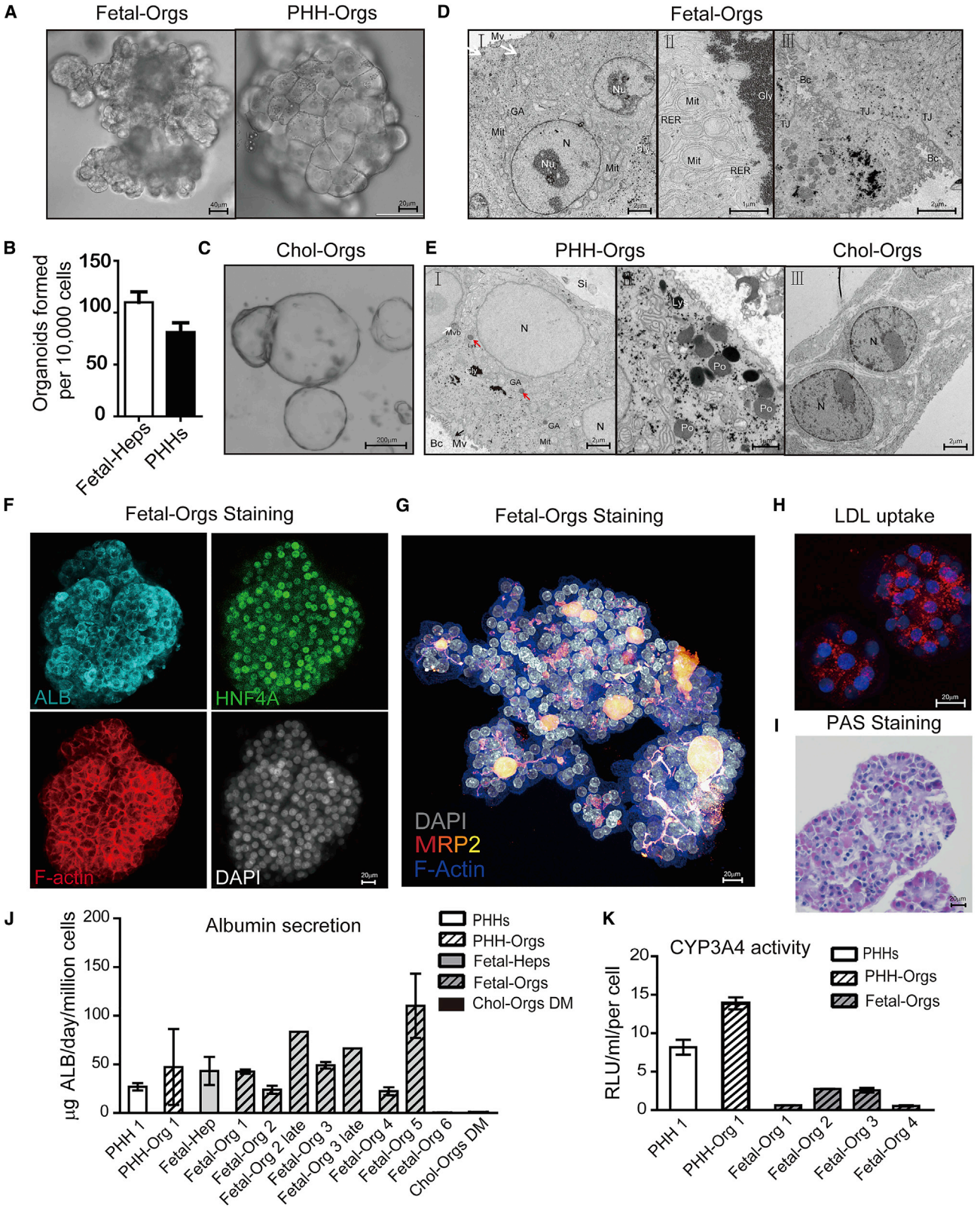

(legend on next page)

but not of Hep-Orgs (Figure S5G). Notably, albumin secretion by Hep-Orgs (6 fetal donors, 1 PHH donor) was comparable to that of PHHs (Figure 5J). A1AT secretion by Hep-Orgs was 25%–50% of the level produced by PHHs (Figure S5H). While ALB slightly increased with increasing Fetal-Org passage number (compare Fetal-Orgs 2 and 3 with Fetal-Orgs 2 late and 3 late in Figure 5J), AFP secretion decreased over time (Figure S5I). CYP3A4 activity in Hep-Orgs derived from PHHs was higher than that of PHHs, while activity in Fetal-Orgs was 2- to 8-fold lower than that of PHHs (Figure 5K).

Bulk mRNA sequencing was performed to compare Fetal-Orgs of different passages and PHH-Orgs to Fetal-Heps and PHHs. The heatmap represents a broad array of hepatocyte genes such as ALB, APOA2 and SERPINA1 in Fetal-Orgs and PHH-Orgs that remained comparable to PHHs over multiple passages (Figure 6A). Expression levels of functional hepatocyte genes (cytochrome P450 activity, glycogen/lipid metabolism and urea cycle) all displayed comparable expression levels between late passage Fetal-Orgs and PHH-Orgs with Fetal-Heps/PHHs (Figure S6A). These levels were much higher than those of hepatocyte-like cells in Chol-Orgs after differentiation. By contrast, progenitor/cholangiocyte markers like EPCAM, SOX9, KRT8/18, and KRT7/19 remained higher in Chol-Orgs in differentiation medium (DM), when compared to Hep-Orgs (Figure S6B). The PCA plot underscored the difference between Chol-Orgs in DM and Hep-Orgs. It is noted that PHH-Orgs re-express AFP (Figure 6A), which makes PHH-Orgs closer to Fetal-Heps than to PHHs in the PCA plot (Figure S6A and Figure S6C).

We then performed single-cell mRNA sequencing on 384 cells derived from Fetal-Orgs and 384 cells from human Chol-Orgs. After applying filtering criteria of a minimum of 4,000 detected transcripts/cell, 161 and 197 cells were retained for analyses, respectively. Clustering analysis by RaceID2 on the combined Fetal-Orgs and Chol-Orgs datasets revealed six main clusters, as visualized in a t-SNE map (Figures 6B and 6C). Cluster i-iv cells almost exclusively derived from Fetal-Orgs. Marker expression analysis (Table S3) revealed that cluster i represented hepatocytes, marked for instance by high Albumin, SERPINA1, and ASGR (Figures 6D–6E and Figure S6D). Cluster ii was defined by mesenchymal markers such as COL1A2 and FSTL1 (Figure S6E). Cluster iii and iv expressed liver progenitor markers such as CD24 and IL32, while some cells were rich in mitochondrial gene mRNAs that are also highly expressed during liver regeneration. The large clusters v and vi expressed (early) cholangiocyte markers such as KRT19 and EPCAM (Figure 6F). Indeed, almost all cells in these two clusters were derived from Chol-Orgs. Both Fetal-Orgs and Chol-Orgs cells expressed markers of proliferation (Figure 6G and Figure S6F).

Human Hep-Orgs Engraft and Repopulate Damaged Mouse Liver

Finally, we addressed whether human Hep-Orgs are able to engraft and repopulate damaged liver tissue. Since transplantability generally correlates with hepatocyte maturity, we defined a differentiation medium (DM, containing dexamethasone and oncostatin M) to increase maturation of Fetal-Orgs (Kamiya et al., 2001) (Figure S7A). Fetal-Org line 2 (Passage 16) cells were seeded on collagen-coated plates for 5–7 days in DM (7–10 days). Subsequently, organoids were transplanted as single cells into immunodeficient *Fah*−/− *NOD Rag1*−/− *Il2rg*−/− (FNRG) mice (Aini et al., 2014; Billerbeck et al., 2016; Grompe, 2017) by splenic injection.

For the first 30 days after transplantation human ALB in mouse circulation remained stable and was clearly detectable in all mice that received Fetal-Orgs (Figure 7D). Initial engraftment of small clusters of 1–2 cells was confirmed by human ALB and NuMa staining (Billerbeck et al., 2016) (Figure 7A). Fetal-Heps of the same donor that were transplanted in parallel as positive control showed continuous increase in hAlb in the same time period and had formed bigger clusters at day 30 post-transplantation. (Figures 7D and S7D). After day 30, however, the organoid graft started to proliferate more rapidly and expanded at the same rate as primary cells. 90 days after transplantation, serum hALB of Fetal-Orgs had risen 200-fold to more than 200 μg/ml on average. Clusters had grown significantly and demonstrated ongoing proliferation as confirmed by Ki67 staining and quantitative histology (Figures 7B and S7B). The repopulating grafts (“nodules”) stained positive for ALB, MRP2 and CYP2E1, which indicated their functional maturity. (Figure 7C) Almost none of the

Figure 5. Establishment of Hep-Orgs from Human Hepatocytes

(A) DIC images of Hep-Orgs from fetal liver on P0 day 21 (Fetal-Orgs, left panel), black scale bar = 40 μm or from primary human hepatocytes (PHHs) on P0 day 19 (PHH-Orgs, right panel), black scale bar = 20 μm.

(B) Numbers of Hep-Orgs formed per 10,000 Fetal-Heps or PHHs. Experiments were performed in triplicate. Data are represented as mean ± SEM.

(C) DIC image showing P5 Chol-Orgs from human adult liver, black scale bar = 200 μm

(D) Transmission EM of Fetal-Orgs (D) I Overview of cell morphology, scale bar = 2 μm; II typical hepatocyte structures, scale Bar = 1 μm; III typical hepatocyte structures, scale bar = 2 μm. N = Nuclear; Nu = Nucleoli, Gly = Glycogen, Mit = Mitochondria, Mv = Microvilli, Tj = Tight junction, GJ = Gap junction, RER = Rough endoplasmic reticulum, Bc = Bile canaliculi-like structures (black arrow), Av = Autophagic vacuoles (white arrow).

(E) Transmission EM of PHH-Orgs and Chol-Orgs (right panel). PHH-Orgs show typical hepatocyte structures. Mvb = Multivesicular bodies, Po = Peroxisomes.

(F) Confocal images of (z stack projection) of human Fetal-Orgs. ALB (cyan), HNF4A (green), F-ACTIN (red), and DAPI (white), scale bale = 20 μm.

(G) Confocal image of whole mount staining of MRP2 and F-ACTIN (3D reconstruction) of human Fetal-Orgs (P26). See also Video S3.

(H) Low density lipoprotein (LDL) uptake was analyzed by Dil-ac-LDL fluorescent staining (red) in cultured human Fetal-Orgs. Nuclei were stained with DAPI (blue). Scale bar = 20 μm.

(I) Glycogen accumulation evaluated by PAS staining (dark pink) in human Fetal-Orgs. Nuclei were stained with hematoxylin (blue). Scale bar = 20 μm.

(J) Albumin secretion by PHHs (white), PHH-Orgs derived from the same PHH batch (white striped), fetal hepatocytes (Fetal-Heps, grey), six independent Fetal Hep-Org cultures (grey striped) and differentiated Chol-Orgs (black). “Late” indicates P22 cultures from one well. Results are indicated as micrograms of albumin per day per million cells. Data are represented as mean ± SEM.

(K) Measurement of cytochrome activity CYP3A4 in PHH-Orgs (striped) compared with PHHs from which they were derived (white) and with four independent Fetal-Org cultures (same numbering as in Figure 5J). Relative light units (RLU) per ml per million cells is given. Data are represented as mean ± SEM.

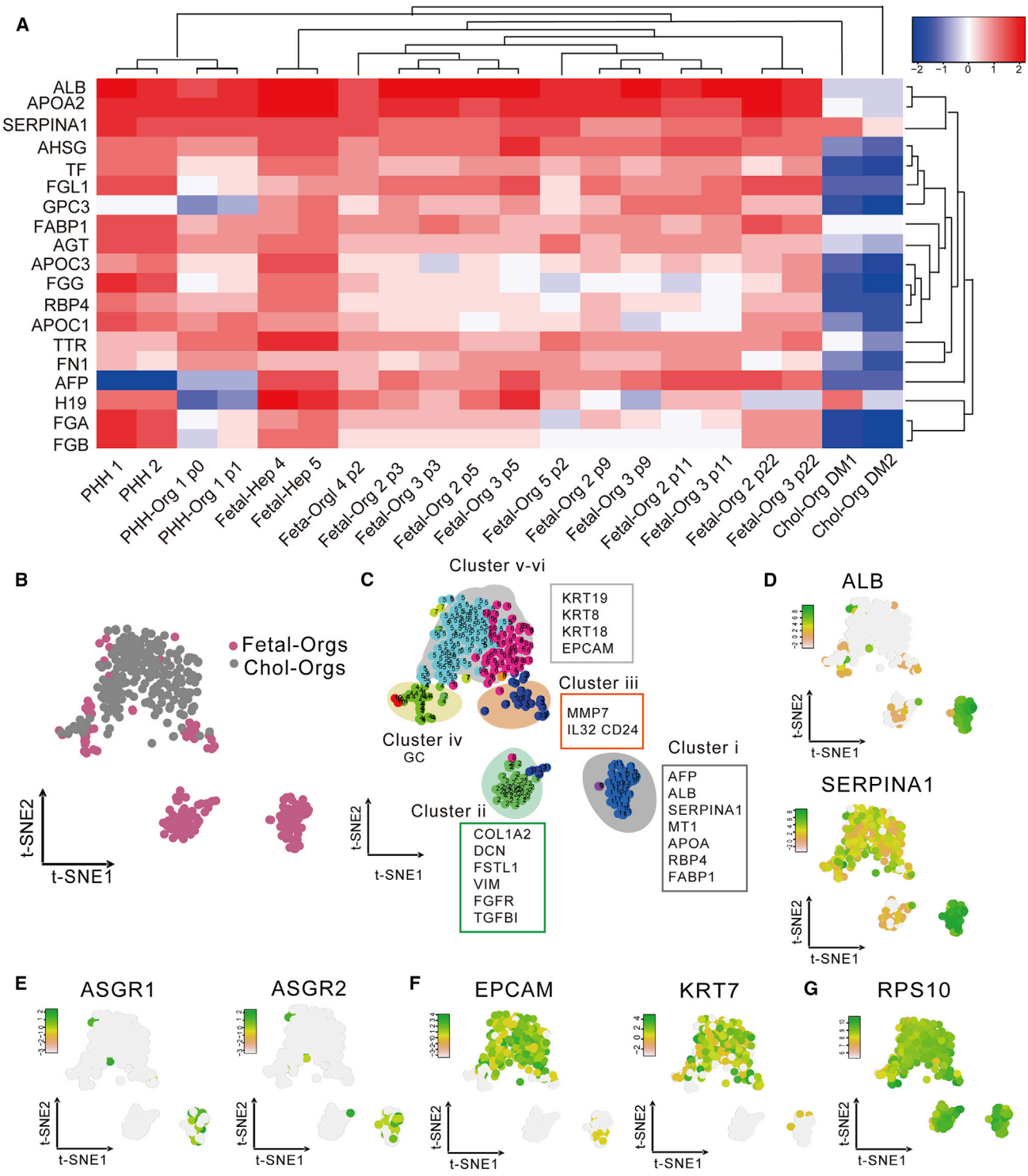

Figure 6. Transcriptional Characterization of Human Hep-Orgs

(A) Heatmap of top expressed hepatic genes in two independent PHH batches, PHH-Orgs, Fetal-Heps, Fetal-Orgs and two differentiated Chol-Orgs. Hep-Org lines labeled as in Figure 5.

(B) t-SNE map combining Fetal-Org cells (purple) with Chol-Org cells (grey).

(C) t-SNE map showing the clustering results of the combined Fetal-Org/Chol-Org dataset. Six main clusters were assigned: Hepatocytes (i), Hepatic mesenchymal-like cells (ii), Progenitors (iii-iv), and Cholangiocytes (v-iv).

(D–G) t-SNE plot emphasizing the expression levels of hepatocyte markers ALB, SERPINA1 (D), ASGR1 and ASGR2 (E), cholangiocyte markers EPCAM and KRT7 (F) and ribosome gene RPS10 (G). Dataset as in Figure 6B. Expression is given as normalized $\log^2$ value.

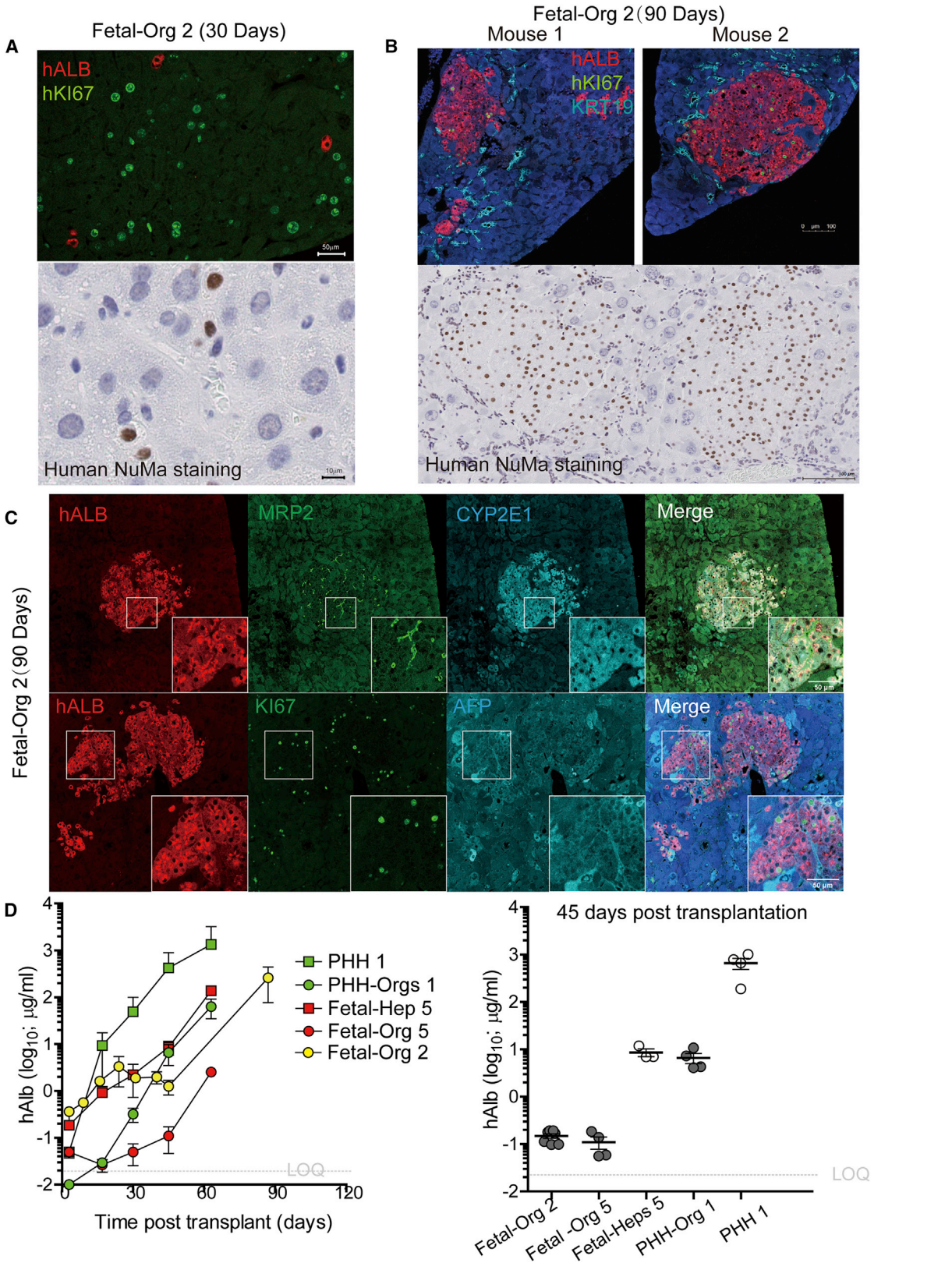

(legend on next page)

transplanted cell retained expression of AFP (fetal hepatocyte marker) and no KRT19 (cholangiocyte marker) could be detected within the graft (Figure 7C and Figure S7C). Encouraged by these results, we attempted the same experiment with an organoid culture grown from one pediatric PHH donor. Since we had access to hepatocytes and Hep-Orgs from the same donor, we were again able to compare engraftment side-by-side. Similar to Fetal-Orgs, mature organoid grafts showed an initial lag phase before proliferating at the same rate as primary hepatocyte controls (Figures 7D and S7D). Mature primary cells and organoids clearly outperformed their fetal counterparts in engraftment level and graft proliferation, which demonstrates the regenerative potential of Hep-Orgs and the faithful conservation of basic tissue features (e.g., transplantability) in organoid culture. In summary, our data show that Hep-Orgs are able to successfully repopulate damaged livers and demonstrate significant graft expansion after transplantation.

DISCUSSION

The ability to culture mature human hepatocytes over long periods of time is key to the development of *in vitro* approaches in toxicology and to the study of hepatotropic infections such as malaria and the hepatitis viruses, and of various hereditary and metabolic liver diseases. Moreover, a better understanding of the basic processes that allow mature hepatocytes to expand would allow the design of novel therapeutic avenues toward regenerative therapy of the liver. Proliferation of adult, functional hepatocytes represents the principle mechanism for replacement of lost liver tissue (Stanger, 2015). It has generally remained challenging to maintain functional, mature hepatocytes in culture for >1–2 weeks, let alone to induce such hepatocytes to enter the cell cycle and to undergo long term expansion *in vitro*.

Co-culture systems or expression of HPV genes have been described to support limited hepatocyte expansion (Khetani and Bhatia, 2008; Levy et al., 2015). Recent efforts have focused on producing hepatocytes *in vitro* by differentiation from pluripotent stem cells (embryonic stem cells or induced pluripotent (iPSCs) (Li et al., 2010a; Liang and Zhang, 2013; Lund et al., 2012). Alternatively, it has been proven feasible to induce trans-differentiation of fibroblasts by transfection with reprogramming genes (Huang et al., 2011; Huang et al., 2014; Swenson, 2012; Zhu et al., 2014). While encouraging results are being reported for these approaches, *in vitro*-produced hepatocyte-like cells do not yet resemble freshly isolated, primary hepatocytes in terms of maturation (Si-Tayeb et al., 2010).

Here, we describe a 3D culture system that allows primary mouse and human hepatocytes to expand for long periods of time. What do we learn from these culture conditions? Activation of the Wnt pathway is one crucial ingredient. This comes as no surprise given that strong Wnt/R-spondin signaling has been implied in hepatocyte proliferation *in vivo* (Planas-Paz et al., 2016; Wang et al., 2015). Moreover, activating Wnt pathway mutations such as in *CTNNB1* occur in hepatocellular carcinomas but are rare in cholangiocyte carcinomas (de La Coste et al., 1998; Marquardt et al., 2015). Another non-surprising component is HGF, a well-known mitogen for hepatocytes (Nakamura et al., 1989). After 2–3 months culturing of murine Hep-Orgs and of human Hep-Orgs derived from adult biopsies, expansion typically slows down. Since we have been able to grow other types of epithelial organoids for >1 year, further improvements to the culture method may be found. One clue may come from our observation that telomeres appear to shorten in liver-derived organoids (H.G. and H.C., unpublished data), a phenomenon that we have not observed in human gut-derived epithelial organoids. Of note, hepatocytes tend to carry relatively short telomeres (Aini et al., 2014; Verma et al., 2012). Interestingly, human hepatocellular carcinomas often harbor activating mutations in the TERT promoter and $TERT^{High}$ hepatocytes have recently been shown to exert a major repopulating activity in response to injury (Lin et al., 2018; Nault et al., 2013), indicating that telomerase activity may be inherently limiting during prolonged adult hepatocyte proliferation. Importantly, the majority of the human Fetal-Org isolates do not seem subject to this slow process of senescence.

The hepatocyte-derived organoids appear to recapitulate the regenerative response of adult liver upon its partial resection. The cultures are initiated from mature hepatocytes and -throughout the culture period- albumin or cytochrome expression remain within the range of primary hepatocytes. Of note, expression of the albumin-related AFP is normally not observed in adult liver but is strongly induced after hemi-hepatectomy; it is also strongly upregulated in Hep-Orgs. The Chol-Orgs that we described previously are very different in terms of cell size, nucleus/cytoplasm ratio, subcellular structure, and function and gene expression profile as determined by single-cell sequencing. Another key difference is the cell-of-origin: Chol-Orgs are grown from EpCAM+ biliary epithelial cells (Huch et al., 2013; Huch et al., 2015). We note the presence of low numbers of cholangiocyte-like cells in hepatocyte organoids and the conversion of Hep-Org cells into Chol-Orgs when transferred to Chol-Org medium *in vitro*. These observations are in agreement with the observed *de novo* generation of bile ducts

Figure 7. Engraftment of Human Hep-Orgs in FNRG Mouse Liver

(A) Human ALB and MKI67 immunofluorescent (top) and human NuMA immunohistochemical (bottom) staining of a representative liver section of an FNRG mouse transplanted with human Fetal-Org cells 30 days after transplantation.

(B) Human ALB, MKI67 and KRT19 immunofluorescent staining (top) and human NuMA immunohistochemical staining (bottom) of a representative liver section of a human Fetal-Org transplanted FNRG mouse 90 days after transplantation.

(C) Human ALB, MRP2, CYP2E1, MKI67 and AFP immunofluorescence staining of a representative liver section of a human Fetal Hep-Org transplanted FNRG mouse 90 days after transplantation.

(D) Left panel compares serum hALB time courses of transplanted PHHs (Primary Human Hepatocytes), transplanted PHH-Orgs (Primary Human Hepatocyte Organoids) and transplanted Fetal Hep-Orgs, with each dot value representing the average of the transplanted group. Right panel: data from the 45 day time point for all mice in each group, where each plot represents one mouse.

after hemi-hepatectomy and the hepatocyte-to-biliary conversion after injury as shown by *in vivo* lineage tracing (Sekiya and Suzuki, 2011). It has been reported that hepatocyte- and cholangiocyte-derived progenitors are functionally different *in vitro*, while hepatocyte-derived progenitors give rise to >60 times more hepatocytes than cholangiocyte-derived progenitors do upon serial transplantation. This suggests that liver cells retain a fate bias during regeneration (Tarlow et al., 2014).

While this work was in progress, we became aware of very similar experiments by Roel Nusse and co-workers (Peng et al., 2018), published elsewhere in this issue, on expanding mouse hepatocyte organoids. Culture conditions are remarkably similar, with the exception of the presence of R-spondin in our cocktal, while the Nusse-study identifies a unique effect of the injury-induced inflammatory cytokine TNFα, for enhanced expansion of hepatocytes. It is obvious that further improvements of culture and transplantation conditions (possibly by combining the two protocols) will be essential steps for potential clinical development.

In conclusion, our culture method for mouse and human hepatocyte organoids recapitulates the proliferative damage-response of liver regeneration and provides a platform for long-term *in vitro* experimentation involving functional hepatocytes.

STAR★METHODS

Detailed methods are provided in the online version of this paper and include the following:

- KEY RESOURCE TABLE
- CONTACT FOR REAGENT AND RESOURCE SHARING
- EXPERIMENTAL MODEL AND SUBJECT DETAILS
  - Mice
  - Cell lines
  - Patients and Clinical Specimens
- METHOD DETAILS
  - Isolation of primary mouse hepatocytes
  - Organoid Culture of Hepatocytes
  - Human Hep-Org Culture
  - RNA isolation and qRT-PCR
  - mRNA Sequencing and Analysis
  - Single-Cell Sequencing and Analysis
  - Immunohistochemistry, Immunofluorescence, Whole Mount Staining and Microscopy
  - Microarray
  - Flow cytometry (FACS)
  - Transmission EM
  - Functional Analysis of Hep-Orgs and Chol-Orgs
  - Transplantation
- QUANTIFICATION AND STATISTICAL ANALYSIS
  - Statistical Analysis
  - GSEA Analysis

SUPPLEMENTAL INFORMATION

Supplemental Information includes seven figures and three tables, and three videos and can be found with this article online at https://doi.org/10.1016/j.cell.2018.11.013.

ACKNOWLEDGMENTS

Thanks to Reinier van der Linden, Stefan van der Elst in FACS facility and Anko de Graaff in Imaging Centre (HIC) of Hubrecht Institute; to Judith Vivié and Mauro Muraro in van Oudenaarden group for single-cell sequencing library and mapping; to the Microscopy Core Lab of M4I Nanoscopy in Maastricht University, in particular to Hans Duimel and Nino Iakobachvili; and to Inha Heo, Marrit Putker Kai Kretzschmar and Georg Busslinger. We sincerely acknowledge all clinical donors. This research was supported by an MKMD grant (114021012) from Netherlands Organization for Scientific Research (NWO-ZonMw), Stichting Vrienden van Hubrecht 2012.10, KNAW 3V-Fund IB/4095 and the Koerber Foundation to H.C.. H.H. was supported by the National Natural Science Foundation of China (31501179), the Foundation for Outstanding Young Scientist in Shandong Province (BS2014SW004) and Future Scientist Program of Chinese Scholarship Council (CSC). H.G. was supported by VENI grant from the NWO-ZonMW 016.166.119. B.A. was supported by fellowship NWO/VENI 863.15.015.

AUTHOR CONTRIBUTIONS

H.H. and H.C. designed the project and wrote the manuscript. H.H. performed most of the experiments including mouse and human hepatocyte organoid establishment, culture, characterizing and analysis. H.G. performed partial hepatectomy, designed transplantation, staining of liver after transplantation and manuscript editing. B.A. did the single-cell sequencing analysis and mRNA sequencing analysis, helped project design and manuscript editing. F.D and A.R. did 3D confocal reconstruction of organoids. O.B. performed mRNA sequencing analysis. J.v.E. and M.v.d.B. bred the mice. H.B. and J.K. performed organoid sections and IHC staining. S.M.C.d.S.L provided the human fetal liver tissue. C.L.-I. and P.J.P. did transmission EM. C.Z., C.Q., L.C., C.M.R and Y.J provided cryopreserved primary human hepatocytes and performed and coordinated chimeric mouse transplantations. S.M. provided micro array data after partial hepatectomy.

DECLARATION OF INTERESTS

H.C. is named is inventor on several patents related to organoids. H.C. is cofounder of and holds stock in Surrozen, Inc.

Received: March 9, 2018
Revised: July 27, 2018
Accepted: November 12, 2018
Published: November 29, 2018

REFERENCES

Aini, W., Miyagawa-Hayashino, A., Ozeki, M., Adeeb, S., Hirata, M., Tamaki, K., Uemoto, S., and Haga, H. (2014). Accelerated telomere reduction and hepatocyte senescence in tolerated human liver allografts. Transpl. Immunol. *31*, 55–59.

Halpern, K.B., Shenhav, R., Matcovitch-Natan, O., Toth, B., Lemze, D., Golan, M., Massasa, E.E., Baydatch, S., Landen, S., Moor, A.E., et al. (2017). Single-cell spatial reconstruction reveals global division of labour in the mammalian liver. Nature *542*, 352–356.

Bartfeld, S., Bayram, T., van de Wetering, M., Huch, M., Begthel, H., Kujala, P., Vries, R., Peters, P.J., and Clevers, H. (2015). In vitro expansion of human gastric epithelial stem cells and their responses to bacterial infection. Gastroenterology *148*, 126–136.e6, e126.

Billerbeck, E., Mommersteeg, M.C., Shlomai, A., Xiao, J.W., Andrus, L., Bhatta, A., Vercauteren, K., Michailidis, E., Dorner, M., Krishnan, A., et al. (2016). Humanized mice efficiently engrafted with fetal hepatoblasts and syngeneic immune cells develop human monocytes and NK cells. J. Hepatol. *65*, 334–343.

Broutier, L., Andersson-Rolf, A., Hindley, C.J., Boj, S.F., Clevers, H., Koo, B.K., and Huch, M. (2016). Culture and establishment of self-renewing human and

mouse adult liver and pancreas 3D organoids and their genetic manipulation. Nat. Protoc. *11*, 1724–1743.

Broutier, L., Mastrogiovanni, G., Verstegen, M.M., Francies, H.E., Gavarró, L.M., Bradshaw, C.R., Allen, G.E., Arnes-Benito, R., Sidorova, O., Gaspersz, M.P., et al. (2017). Human primary liver cancer-derived organoid cultures for disease modeling and drug screening. Nat. Med. *23*, 1424–1435.

Burke, Z.D., Reed, K.R., Phesse, T.J., Sansom, O.J., Clarke, A.R., and Tosh, D. (2009). Liver zonation occurs through a beta-catenin-dependent, c-Myc-independent mechanism. Gastroenterology *136*, 2316–2324.e2311–2313.

de La Coste, A., Romagnolo, B., Billuart, P., Renard, C.A., Buendia, M.A., Soubrane, O., Fabre, M., Chelly, J., Beldjord, C., Kahn, A., and Perret, C. (1998). Somatic mutations of the beta-catenin gene are frequent in mouse and human hepatocellular carcinomas. Proc. Natl. Acad. Sci. USA *95*, 8847–8851.

Dollé, L., Theise, N.D., Schmelzer, E., Boulter, L., Gires, O., and van Grunsven, L.A. (2015). EpCAM and the biology of hepatic stem/progenitor cells. Am. J. Physiol. Gastrointest. Liver Physiol. *308*, G233–G250.

Drost, J., Karthaus, W.R., Gao, D., Driehuis, E., Sawyers, C.L., Chen, Y., and Clevers, H. (2016). Organoid culture systems for prostate epithelial and cancer tissue. Nat. Protoc. *11*, 347–358.

Duncan, A.W., Taylor, M.H., Hickey, R.D., Hanlon Newell, A.E., Lenzi, M.L., Olson, S.B., Finegold, M.J., and Grompe, M. (2010). The ploidy conveyor of mature hepatocytes as a source of genetic variation. Nature *467*, 707–710.

Engelhardt, N.V., Lazareva, M.N., Abelev, G.I., Uryvaeva, I.V., Factor, V.M., and Brodsky, V.Y. (1976). Detection of alpha-foetoprotein in mouse liver differentiated hepatocytes before their progression through S phase. Nature *263*, 146–148.

Evarts, R.P., Nagy, P., Marsden, E., and Thorgeirsson, S.S. (1987). A precursor-product relationship exists between oval cells and hepatocytes in rat liver. Carcinogenesis *8*, 1737–1740.

Fan, B., Malato, Y., Calvisi, D.F., Naqvi, S., Razumilava, N., Ribback, S., Gores, G.J., Dombrowski, F., Evert, M., Chen, X., and Willenbring, H. (2012). Cholangiocarcinomas can originate from hepatocytes in mice. J. Clin. Invest. *122*, 2911–2915.

Font-Burgada, J., Shalapour, S., Ramaswamy, S., Hsueh, B., Rossell, D., Umemura, A., Taniguchi, K., Nakagawa, H., Valasek, M.A., Ye, L., et al. (2015). Hybrid Periportal Hepatocytes Regenerate the Injured Liver without Giving Rise to Cancer. Cell *162*, 766–779.

Furuyama, K., Kawaguchi, Y., Akiyama, H., Horiguchi, M., Kodama, S., Kuhara, T., Hosokawa, S., Elbahrawy, A., Soeda, T., Koizumi, M., et al. (2011). Continuous cell supply from a Sox9-expressing progenitor zone in adult liver, exocrine pancreas and intestine. Nat. Genet. *43*, 34–41.

Greene, A.K., and Puder, M. (2003). Partial hepatectomy in the mouse: technique and perioperative management. J. Invest. Surg. *16*, 99–102.

Grompe, M. (2014). Liver stem cells, where art thou? Cell Stem Cell *15*, 257–258.

Grompe, M. (2017). Fah Knockout Animals as Models for Therapeutic Liver Repopulation. Adv. Exp. Med. Biol. *959*, 215–230.

Grün, D., Lyubimova, A., Kester, L., Wiebrands, K., Basak, O., Sasaki, N., Clevers, H., and van Oudenaarden, A. (2015). Single-cell messenger RNA sequencing reveals rare intestinal cell types. Nature *525*, 251–255.

Hashimshony, T., Senderovich, N., Avital, G., Klochendler, A., de Leeuw, Y., Anavy, L., Gennert, D., Li, S., Livak, K.J., Rozenblatt-Rosen, O., et al. (2016). CEL-Seq2: sensitive highly-multiplexed single-cell RNA-Seq. Genome Biol. *17*, 77.

Huang, P., He, Z., Ji, S., Sun, H., Xiang, D., Liu, C., Hu, Y., Wang, X., and Hui, L. (2011). Induction of functional hepatocyte-like cells from mouse fibroblasts by defined factors. Nature *475*, 386–389.

Huang, P., Zhang, L., Gao, Y., He, Z., Yao, D., Wu, Z., Cen, J., Chen, X., Liu, C., Hu, Y., et al. (2014). Direct reprogramming of human fibroblasts to functional and expandable hepatocytes. Cell Stem Cell *14*, 370–384.

Huch, M., and Clevers, H. (2011). Sox9 marks adult organ progenitors. Nat. Genet. *43*, 9–10.

Huch, M., Dorrell, C., Boj, S.F., van Es, J.H., Li, V.S., van de Wetering, M., Sato, T., Hamer, K., Sasaki, N., Finegold, M.J., et al. (2013). In vitro expansion of single Lgr5+ liver stem cells induced by Wnt-driven regeneration. Nature *494*, 247–250.

Huch, M., Gehart, H., van Boxtel, R., Hamer, K., Blokzijl, F., Verstegen, M.M., Ellis, E., van Wenum, M., Fuchs, S.A., de Ligt, J., et al. (2015). Long-term culture of genome-stable bipotent stem cells from adult human liver. Cell *160*, 299–312.

Kamiya, A., Kinoshita, T., and Miyajima, A. (2001). Oncostatin M and hepatocyte growth factor induce hepatic maturation via distinct signaling pathways. FEBS Lett. *492*, 90–94.

Katsuda, T., Kawamata, M., Hagiwara, K., Takahashi, R.U., Yamamoto, Y., Camargo, F.D., and Ochiya, T. (2017). Conversion of Terminally Committed Hepatocytes to Culturable Bipotent Progenitor Cells with Regenerative Capacity. Cell Stem Cell *20*, 41–55.

Khetani, S.R., and Bhatia, S.N. (2008). Microscale culture of human liver cells for drug development. Nat. Biotechnol. *26*, 120–126.

Levy, G., Bomze, D., Heinz, S., Ramachandran, S.D., Noerenberg, A., Cohen, M., Shibolet, O., Sklan, E., Braspenning, J., and Nahmias, Y. (2015). Long-term culture and expansion of primary human hepatocytes. Nat. Biotechnol. *33*, 1264–1271.

Li, B., Dorrell, C., Canaday, P.S., Pelz, C., Haft, A., Finegold, M., and Grompe, M. (2017). Adult Mouse Liver Contains Two Distinct Populations of Cholangiocytes. Stem Cell Reports *9*, 478–489.

Li, F., Liu, P., Liu, C., Xiang, D., Deng, L., Li, W., Wangensteen, K., Song, J., Ma, Y., Hui, L., et al. (2010a). Hepatoblast-like progenitor cells derived from embryonic stem cells can repopulate livers of mice. Gastroenterology *139*, 2158–2169 e2158.

Li, W.C., Ralphs, K.L., and Tosh, D. (2010b). Isolation and culture of adult mouse hepatocytes. Methods Mol. Biol. *633*, 185–196.

Liang, G., and Zhang, Y. (2013). Genetic and epigenetic variations in iPSCs: potential causes and implications for application. Cell Stem Cell *13*, 149–159.

Lin, S., Nascimento, E.M., Gajera, C.R., Chen, L., Neuhöfer, P., Garbuzov, A., Wang, S., and Artandi, S.E. (2018). Distributed hepatocytes expressing telomerase repopulate the liver in homeostasis and injury. Nature *556*, 244–248.

Liu, Y., Cao, L., Chen, R., Zhou, X., Fan, X., Liang, Y., Jia, R., Wang, H., Liu, G., Guo, Y., and Zhao, J. (2015). Osteopontin Promotes Hepatic Progenitor Cell Expansion and Tumorigenicity via Activation of β-Catenin in Mice. Stem Cells *33*, 3569–3580.

Love, M.I., Huber, W., and Anders, S. (2014). Moderated estimation of fold change and dispersion for RNA-seq data with DESeq2. Genome Biol. *15*, 550.

Lund, R.J., Närvä, E., and Lahesmaa, R. (2012). Genetic and epigenetic stability of human pluripotent stem cells. Nat. Rev. Genet. *13*, 732–744.

Madisen, L., Zwingman, T.A., Sunkin, S.M., Oh, S.W., Zariwala, H.A., Gu, H., Ng, L.L., Palmiter, R.D., Hawrylycz, M.J., Jones, A.R., et al. (2010). A robust and high-throughput Cre reporting and characterization system for the whole mouse brain. Nat Neurosci. *13*, 133–140.

Malato, Y., Naqvi, S., Schürmann, N., Ng, R., Wang, B., Zape, J., Kay, M.A., Grimm, D., and Willenbring, H. (2011). Fate tracing of mature hepatocytes in mouse liver homeostasis and regeneration. J. Clin. Invest. *121*, 4850–4860.

Marquardt, J.U., Andersen, J.B., and Thorgeirsson, S.S. (2015). Functional and genetic deconstruction of the cellular origin in liver cancer. Nat. Rev. Cancer *15*, 653–667.

Michalopoulos, G.K. (2010). Liver regeneration after partial hepatectomy: critical analysis of mechanistic dilemmas. Am. J. Pathol. *176*, 2–13.

Miyajima, A., Tanaka, M., and Itoh, T. (2014). Stem/progenitor cells in liver development, homeostasis, regeneration, and reprogramming. Cell Stem Cell *14*, 561–574.

Nakamura, T., Nishizawa, T., Hagiya, M., Seki, T., Shimonishi, M., Sugimura, A., Tashiro, K., and Shimizu, S. (1989). Molecular cloning and expression of human hepatocyte growth factor. Nature *342*, 440–443.

Nault, J.C., Mallet, M., Pilati, C., Calderaro, J., Bioulac-Sage, P., Laurent, C., Laurent, A., Cherqui, D., Balabaud, C., and Zucman-Rossi, J. (2013). High frequency of telomerase reverse-transcriptase promoter somatic mutations in hepatocellular carcinoma and preneoplastic lesions. Nat. Commun. *4*, 2218.

Peng, W.C., Logan, C.Y., Fish, M., Anbarchian, T., Aguisanda, F., Álvarez-Varela, A., Wu, P., Jin, Y., Zhu, J., Li, B., et al. (2018). Inflammatory Cytokine TNFα Promotes the Expansion of Primary Hepatocytes in 3D Culture. Cell *175*. Published online November 29, 2018. https://doi.org/10.1016/j.cell.2018.11.012.

Planas-Paz, L., Orsini, V., Boulter, L., Calabrese, D., Pikiolek, M., Nigsch, F., Xie, Y., Roma, G., Donovan, A., Marti, P., et al. (2016). The RSPO-LGR4/5-ZNRF3/RNF43 module controls liver zonation and size. Nat. Cell Biol. *18*, 467–479.

Raven, A., Lu, W.Y., Man, T.Y., Ferreira-Gonzalez, S., O'Duibhir, E., Dwyer, B.J., Thomson, J.P., Meehan, R.R., Bogorad, R., Koteliansky, V., et al. (2017). Cholangiocytes act as facultative liver stem cells during impaired hepatocyte regeneration. Nature *547*, 350–354.

Sato, T., Stange, D.E., Ferrante, M., Vries, R.G., Van Es, J.H., Van den Brink, S., Van Houdt, W.J., Pronk, A., Van Gorp, J., Siersema, P.D., and Clevers, H. (2011). Long-term expansion of epithelial organoids from human colon, adenoma, adenocarcinoma, and Barrett's epithelium. Gastroenterology *141*, 1762–1772.

Schaub, J.R., Malato, Y., Gormond, C., and Willenbring, H. (2014). Evidence against a stem cell origin of new hepatocytes in a common mouse model of chronic liver injury. Cell Rep. *8*, 933–939.

Schuler, M., Dierich, A., Chambon, P., and Metzger, D. (2004). Efficient temporally controlled targeted somatic mutagenesis in hepatocytes of the mouse. Genesis *39*, 167–172.

Sekiya, S., and Suzuki, A. (2011). Direct conversion of mouse fibroblasts to -hepatocyte-like cells by defined factors. Nature *475*, 390–393.

Sekiya, S., and Suzuki, A. (2014). Hepatocytes, rather than cholangiocytes, can be the major source of primitive ductules in the chronically injured mouse liver. Am. J. Pathol. *184*, 1468–1478.

Sell, S., Nichols, M., Becker, F.F., and Leffert, H.L. (1974). Hepatocyte proliferation and alpha 1-fetoprotein in pregnant, neonatal, and partially hepatectomized rats. Cancer Res. *34*, 865–871.

Si-Tayeb, K., Noto, F.K., Nagaoka, M., Li, J., Battle, M.A., Duris, C., North, P.E., Dalton, S., and Duncan, S.A. (2010). Highly efficient generation of human hepatocyte-like cells from induced pluripotent stem cells. Hepatology *51*, 297–305.

Stanger, B.Z. (2015). Cellular homeostasis and repair in the mammalian liver. Annu. Rev. Physiol. *77*, 179–200.

Swenson, E.S. (2012). Direct conversion of mouse fibroblasts to hepatocyte-like cells using forced expression of endodermal transcription factors. Hepatology *55*, 316–318.

Tanimizu, N., Nishikawa, Y., Ichinohe, N., Akiyama, H., and Mitaka, T. (2014). Sry HMG box protein 9-positive (Sox9+) epithelial cell adhesion molecule-negative (EpCAM-) biphenotypic cells derived from hepatocytes are involved in mouse liver regeneration. J. Biol. Chem. *289*, 7589–7598.

Tarlow, B.D., Pelz, C., Naugler, W.E., Wakefield, L., Wilson, E.M., Finegold, M.J., and Grompe, M. (2014). Bipotential adult liver progenitors are derived from chronically injured mature hepatocytes. Cell Stem Cell *15*, 605–618.

van Amerongen, R., Bowman, A.N., and Nusse, R. (2012). Developmental stage and time dictate the fate of Wnt/β-catenin-responsive stem cells in the mammary gland. Cell Stem Cell *11*, 387–400.

Verma, S., Tachtatzis, P., Penrhyn-Lowe, S., Scarpini, C., Jurk, D., Von Zglinicki, T., Coleman, N., and Alexander, G.J. (2012). Sustained telomere length in hepatocytes and cholangiocytes with increasing age in normal liver. Hepatology *56*, 1510–1520.

Wang, B., Zhao, L., Fish, M., Logan, C.Y., and Nusse, R. (2015). Self-renewing diploid Axin2(+) cells fuel homeostatic renewal of the liver. Nature *524*, 180–185.

Yanger, K., Knigin, D., Zong, Y., Maggs, L., Gu, G., Akiyama, H., Pikarsky, E., and Stanger, B.Z. (2014). Adult hepatocytes are generated by self-duplication rather than stem cell differentiation. Cell Stem Cell *15*, 340–349.

Yanger, K., Zong, Y., Maggs, L.R., Shapira, S.N., Maddipati, R., Aiello, N.M., Thung, S.N., Wells, R.G., Greenbaum, L.E., and Stanger, B.Z. (2013). Robust cellular reprogramming occurs spontaneously during liver regeneration. Genes Dev. *27*, 719–724.

Yimlamai, D., Christodoulou, C., Galli, G.G., Yanger, K., Pepe-Mooney, B., Gurung, B., Shrestha, K., Cahan, P., Stanger, B.Z., and Camargo, F.D. (2014). Hippo pathway activity influences liver cell fate. Cell *157*, 1324–1338.

Yokoyama, H.O., Wilson, M.E., Tsuboi, K.K., and Stowell, R.E. (1953). Regeneration of mouse liver after partial hepatectomy. Cancer Res. *13*, 80–85.

Zhu, S., Rezvani, M., Harbell, J., Mattis, A.N., Wolfe, A.R., Benet, L.Z., Willenbring, H., and Ding, S. (2014). Mouse liver repopulation with hepatocytes generated from human fibroblasts. Nature *508*, 93–97.

STAR★METHODS

KEY RESOURCE TABLE

REAGENT or RESOURCE	SOURCE	IDENTIFIER
Antibodies		
Anti-Mouse Albumin	Santa cruz	Cat#Sc-46291; RRID: AB_633768
Anti-Human ALBUMIN	Bethyl	Cat#A80-229A; RRID: AB_67018
Anti-Mouse/HUMAN Ki67	Abcam	Cat#ab16667; RRID: AB_302459
Anti-Human KI67	BD	Cat#550609; RRID: AB_393778
Anti-KRT7	Thermo	Cat#180234; RRID: AB_86727
Anti-Krt19	Cell Signaling	Cat#4558S; RRID: AB_2133445
Anti-GLT1	Abcam	Cat#ab41621; RRID: AB_941782
Anti-Epcam	eBioscience	Cat#17-5791-82; RRID: AB_2716944
Anti-EPCAM	Biolegend	Cat#324210; RRID: AB_756084
Anti-CDH1	BD	Cat#610182; RRID: AB_397581
Anti-CTNNB1(mouse)	BD	Cat#610154; RRID: AB_397555
Anti-CTNNB1(rabbit)	Santa cruz	Cat#Sc-7199; RRID: AB_634603
Anti-HNF4A	Santa cruz	Cat#Sc-8987; RRID: AB_2116913
Anti-HNF4A	Thermo	Cat#MA1-199; RRID: AB_2633309
Anti-CYP2E1	Abnova	Cat#PAB11973; RRID: AB_1672669
Anti-AFP	Thermo	Cat#PA5-16658; RRID:AB_10979157
Anti-NuMa	Abcam	Cat#ab97585; RRID:AB_10680001
Anti- Glutamine synthetase	BD	Cat#610517; RRID:AB_2313837
Anti-RFP/Tomato	Rockland	Cat#600-401-379; RRID:AB_2209751
Anti-FACTIN	Thermo	Cat#A22287; RRID:AB_2620155
Anti-MRP2	Abcam	Cat#A80-122A; RRID:AB_67027
Chemicals, Peptides, and Recombinant Proteins		
TRIzol	Thermo	15596-018
Matrigel (BME)	AMSBIO	3533-005-02
Hepes	Thermo	15630-056
GlutaMax	Thermo	35050-038
Penicillin-Streptomycin	Thermo	15140-122
EGF	Peprotech	AF-100-15
TGFa	Peprotech	239-A-100
FGF7	Peprotech	100-19-100?g
FGF10	Peprotech	100-26-100?g
CHIR	Tocris	CAS#252917-06-9
N-Acetylcysteine	Sigma-Aldrich	A9165
Gastrin	Tocris	3006
Nicotinamide	Sigma-Aldrich	N0636
HGF	Peprotech	100-39-100?g
B27 Supplement (minus Vitamin A)	Thermo	12587-010
A83-01	Tocris	2939
γ-27632	Abmole	M1817
Primocin	InvivoGen	Ant-pm-1
Dexamethasone	Sigma-Aldrich	D4902

(*Continued on next page*)

Continued

REAGENT or RESOURCE	SOURCE	IDENTIFIER
Oncostatin M	R&D	295OM
DAPI	Thermo	D1306
Critical Commercial Assays		
Di-Ac-Ldl	Biomedical technologogies	BT-902
Rhodamine 123	Thermo	R302
Cytochrome activity kit	CYP3A4 Assay	V8901
Mouse Alb Elisa kit	Bethyl	E99-134
Human ALB Elisa kit	Bethyl	E88-129
Human α1-Antitrypsin Elisa kit	Assaypro	EA5101-1
Human alpha-Fetoprotein ELISA Kit	R&D systems	DAFP00
CellTiter-Glo® 3D Cell Viability Assay	Promega	G9682
Thermo Scientific reagents for CEL-Seq2	Hashimshony et al., 2016	N/A
Deposited Data		
Raw and analyzed sequencing and microarray data	This paper	GSE111301 and GSE110292
Experimental Models: Organisms/Strains		
C57B6	Jackson lab	000664
BALB/c	Jackson lab	000651
Axin2-CreERT2	Jackson lab	018867
Albumin-CreERT2	Jackson lab	MGI:3052812
Rosa26-LSL-tdTomato	Madisen et al., 2010	007909
Software and Algorithms		
Prism Graphpad 5.0		Graphpad Software
Adobe photoshop CS4	Adobe	https://adobe-photoshop.en.softonic.com/windows/download
Adobe illustator	Adobe	http://www.adobe.com/products/illustrator.html
Image J	NIH	https://imagej.nih.gov/ij/
Rtudio	Rstudio	https://www.rstudio.com/
Oligonucleotides		
Primer: Afp Forward for total mouse cDNA: CCAGGA AGTCTGTTTCACAGAAG	This paper	N/A
Primer: Afp Reverse for total mouse cDNA: CAAAAG GCTCACACCAAAGAG	This paper	N/A
Primer: Alb Forward for total mouse cDNA: AGCCCA CTGTCTTAGTGAGG	This paper	N/A
Primer: Alb Reverse for total mouse cDNA: TCTTGC ACACTTCCTGGTCC	This paper	N/A
Primer: Hnf4a Forward for total mouse cDNA: GCTA AGGCGTGGGTAGGG	This paper	N/A
Primer: Hnf4a Reverse for total mouse cDNA: AGGC TGTTGGATGAATTGAGG	This paper	N/A
Primer: Cyp1a2 Forward for total mouse cDNA: TTC AGTCCCTCCTTACAGCC	This paper	N/A
Primer: Cyp1a2 Reverse for total mouse cDNA: TCC AAGGCAGAATACGGTGAC	This paper	N/A
Primer: Cyp3a11 Forward for total mouse cDNA: TGG TCAAACGCCTCTCCTTGCTG	This paper	N/A
Primer: Cyp3a11 Reverse for total mouse cDNA: ACT GGGCCAAAATCCCGCCG	This paper	N/A

(*Continued on next page*)

Continued

REAGENT or RESOURCE	SOURCE	IDENTIFIER
Primer: Krt19 Forward for total mouse cDNA: GTCCTA CAGATTGACAATGC	This paper	N/A
Primer: Krt19 Reverse for total mouse cDNA: CACGC TCTGGATCTGTGACA	This paper	N/A
Primer: Tbx3 Forward for total mouse cDNA: GAGGC CAAGGAACTTTGGGA	This paper	N/A
Primer: Tbx3 Reverse for total mouse cDNA: AGGGA ACATTCGCCTTCCTG	This paper	N/A
Primer: Sox9 Forward for total mouse cDNA: TGCTG GTGTGGTGAAAGGTT	This paper	N/A
Primer: Sox9 Reverse for total mouse cDNA: CCAGG AGCAACAAAGTTGGC	This paper	N/A
Primer: Arg1 Forward for total mouse cDNA: GAGCTC CAAGCCAAAGTCCT	This paper	N/A
Primer: Arg1 Reverse for total mouse cDNA: GGTCTC TCACGTCATACTCTGTT	This paper	N/A
Primer: Cps1 Forward for total mouse cDNA: GCCAAT GTGACTACGAAGCG	This paper	N/A
Primer: Cps1 Reverse for total mouse cDNA: TTCCGG GTACCCTCCTAAGC	This paper	N/A
Primer: Pck1 Forward for total mouse cDNA: ATGAAA GGCCGCACCATGTA	This paper	N/A
Primer: Pck1 Reverse for total mouse cDNA: GGGCG AGTCTGTCAGTTCAA	This paper	N/A
Primer: Axin2 Forward for total mouse cDNA: TAAGCA GCCGTTCGCGATG	This paper	N/A
Primer: Axin2 Reverse for total mouse cDNA: TTCTTC CAGTTCCTCTCAG	This paper	N/A
Primer: Gstm3 Forward for total mouse cDNA: TGCT GGTGTGGTGAAAGGTT	This paper	N/A
Primer: Gstm3 Reverse for total mouse cDNA: CCAG GAGCAACAAAGTTGGC	This paper	N/A
Primer: Aat Forward for total mouse cDNA: TCAAACC AGAAAACGGAAGC	This paper	N/A
Primer: Aat Reverse for total mouse cDNA: CTGCTGT GCCCATAGTGAGA	This paper	N/A
Primer: Glu Forward for total mouse cDNA: AAGATCA TTGGCGGAAAG	This paper	N/A
Primer: Glu Reverse for total mouse cDNA: GAGTGCT CAGGATGTTAAG	This paper	N/A
Primer: Gapdh Forward for total mouse cDNA: ATGGT GAAGGTCGGTGTGAAC	This paper	N/A
Primer: Gapdh Reverse for total mouse cDNA: GCCGT GAGTGGAGTCATACTG	This paper	N/A

CONTACT FOR REAGENT AND RESOURCE SHARING

Further information and requests for resources and reagents should be directed to the Lead Contact, Hans Clevers (h.clevers@hubrecht.eu).

EXPERIMENTAL MODEL AND SUBJECT DETAILS

Mice

All animal experiments were performed after institutional review by the Animal Ethics Committee of the Royal Netherlands Academy of Arts and Sciences (KNAW) with project license of AVD8010020151 and research protocol HI16.10.05 and HI16.1002. Albumin-Cre^{ERT2} and Axin2-Cre^{ERT2} mice were described before (Schuler et al., 2004; van Amerongen et al., 2012). Rosa26-LSL-tdTomato mice were crossed with Albumin-Cre^{ERT2} or Axin2-Cre^{ERT2} mice and their offspring were used for lineage tracing. Generation and genotyping methods have been previously described (Schuler et al., 2004; van Amerongen et al., 2012). Mice carrying Cre and Rosa alleles aged 8–24 weeks were subjected to a single intraperitoneal injection of 0.2mg per 25 g of body weight tamoxifen (Sigma, T548). Mice were collected after 5–7 days after induction. Both male and female mice were used. For PHx, surgery was performed as described (Greene and Puder, 2003). Mice were sacrificed 2.5–3 days post-PHx (Greene and Puder, 2003; Yokoyama et al., 1953). For human cell transplantations, *Fah*$^{-/-}$ NOD *Rag1*$^{-/-}$ *Il2rg*^{null} (FNRG) female mice were used at the Rockefeller University under IACUC protocol 15814.

Cell lines

293t-HA-Rspon1-Fc cells were used as previously described to generate conditional medium of R-spondin1. Cells were cultured in a humidified 5% CO2 atmosphere. Commercial human primary hepatocytes were obtained from Thermo Scientific (HMCS10).

Patients and Clinical Specimens

Human fetal livers were obtained from Susana M. Chuva de Sousa Lopes in Leiden University Medical Center. Human liver biopsies were obtained from patients undergoing surgery at University Medical Centre Utrecht Hospital and Rotterdam and University Medical Center. Human cryopreserved fetal and primary human hepatocytes were from Rockefeller University and Lonza Company. The use of samples for research was approved by ethical committees and informed consent were obtained from donors when appropriate.

METHOD DETAILS

Isolation of primary mouse hepatocytes

Hepatocytes were isolated from mice by two-step collagenase perfusion (Li et al., 2010b). Briefly, after placing catheter into the portal vein, the inferior vena cava was cut and the liver was perfused at 5–7 ml/min with pre-warmed Perfusion Medium for 10 minutes. Then, perfusion was performed with pre-warmed Digestion Medium including Type IV collagenase and Ca^{2+} at 5 ml/min for 3–5 minutes. After dissociation, cells were filtered through a 70 μm filter. Hepatocytes were further separated and purified by centrifugation at low speed (50 g, 1–3min) and Percoll gradient centrifugation was optimally performed as described before (Broutier et al., 2016; Huch et al., 2013) .

Organoid Culture of Hepatocytes

Isolated hepatocytes were filtered by 70 μm filter, washed twice with cold AdDMEM/F12, counted and mixed with Matrigel in suspension plates (Greiner). 20,000–50,000 cells were used per well of a 24 well plate. After Matrigel was solidified, Hep-Medium was added. Hep-Medium consists of AdDMEM/F12 (Thermo Scientific, with HEPES, GlutaMax and Penicillin-Streptomycin) plus 15% RSPO1 conditioned medium (home-made), B27 (minus vitamin A), 50ng/ml EGF (Peprotech), 1.25mM N-acetylcysteine (Sigma), 10 nM gastrin (Sigma), 3 μm CHIR99021 (Sigma), 25ng/ml HGF (Peprotech), 50ng/ml FGF7 (Peprotech), 50ng/ml FGF10 (Peprotech), 1 μM A83-01 (Tocris), 10 mM Nicotinamide (Sigma), and 10 μM Rho Inhibitor γ-27632 (Calbiochem). 14 days after seeding, organoids were mechanically fragmented and re-seeded into new Matrigel. During culturing, medium was refreshed at most every three days. Organoids are usually passaged with a split ratio of 1:3 every 7–10 days.

Human Hep-Org Culture

Fetal hepatocytes were isolated from human fetal tissue by the two-step collagenase perfusion method and isolated by 5min centrifugation at 100 g. Red blood cells were removed. Hepatocytes were isolated from human adult liver by two steps of collagenase digestion and cells were filtered through a 70 μm filter and collected by 5min centrifugation at 100 g. Different fractions were washed with Advanced DMEM/F12. 10,000 cryopreserved fetal (11–20 weeks), pediatric (age = 0.6 years) and adult hepatocytes or freshly isolated cells were mixed with human Hep-Medium and Matrigel (with a ratio of 1:3) and seeded per 24 wells. After solidification, medium was added. Human Hep-Medium: AdDMEM/F12 (Thermo Scientific, with HEPES, GlutaMax and Penicillin-Streptomycin) plus 15% RSPO1 conditioned medium (home-made), B27 (minus vitamin A), 50ng/ml EGF (Peprotech), 1.25mM N-acetylcysteine (Sigma), 10 nM gastrin (Sigma), 3 μm CHIR99021 (Sigma), 50ng/ml HGF (Peprotech), 100ng/ml FGF7 (Peprotech), 100ng/ml FGF10 (Peprotech), 2 μM A83-01 (Tocris), 10 mM Nicotinamide (Sigma), 10 μM Rho Inhibitor γ-27632 (Calbiochem) and 20ng/ml TGFa. For Fetal-Org differentiation, Human Hep-Medium was supplemented with 10ng/ml Oncostatin M and 1 μM Dexamethasone (Differentiation Medium, DM). During culturing, medium was refreshed every 2–3 days. Organoids are usually passaged with a split ratio of 1:3 every 7–8 days until P10-15 and 1:3 every 14 days from P15 onward. Chol-Orgs were cultured and passaged as previously

described (Broutier et al., 2016). Cell number of organoids growth was calculated by CellTiter-Glo® 3D Cell Viability Assay with a standard curve made from known numbers of primary hepatocytes.

RNA isolation and qRT-PCR

RNA isolation of organoids, tissues, and primary cells were performed with RNeasy Mini Kit (QIAGEN) following the manufacturer's instructions. Samples with low amount of RNA were lysed in TRIzol (Invitrogen). RNA was reverse transcribed with M-MLV Reverse Transcriptase, RNase H Minus (Promega). qPCR analysis was performed with SYBR Green Mixture (Bio-rad Laboratories) in 96 or 384 q-PCR machine (Bio-rad Laboratories). Primers for qPCR were designed using NCBI Primer-BLAST and are listed in Key Resource Table.

mRNA Sequencing and Analysis

RNA-sequencing libraries were prepared based on the DESeq2 method (Hashimshony et al., 2016; Love et al., 2014). Briefly, total mRNA was isolated by TRIzol or RNeasy Mini Kit (QIAGEN) and reverse transcribed with Ambion kit. *In vitro* transcription was performed using 1–5 ng cDNA as template and RNA was reverse transcribed into sequencing library. Samples were sequenced on an Illumina HiSeq 2000 instrument. Sequencing data analysis was performed using the DESeq2 package (CIT) in R environment. Paired reads were then quantified and normalized. Sample variability was visualized by Principal Component Analysis (PCA). Differential gene expression analysis was performed by DeSeq2 package and visualized by heatmap. Correlation analysis and visualization was performed with Corrplot package. All data analysis and visualization were performed suing R studio.

Single-Cell Sequencing and Analysis

Organoids were trypsinized and tissue was perfused with collagenase into single cells. DAPI was used for live/dead cell discrimination. Single, live cells were sorted in 384-well plates using an Aria II cell sorter (BD bioscience). Sequencing library were prepared accordingly to CEL-seq2 methods (Hashimshony et al., 2016). Briefly, after sorting into 384 plates, cells were lysed at 65°C for 5 minutes and then RNAs were reverse transcribed and pooled before *in vitro* transcription. Illumina sequencing libraries were prepared using the TruSeq small RNA primers (Illumina) and sequenced paired-end at 75 bp read length on Illumina NextSeq500. All data analysis was performed using RaceID2 algorithm. All RNA sequencing data are accessible through GEO: GSE111301 in the NCBI Gene Expression Omnibus

Immunohistochemistry, Immunofluorescence, Whole Mount Staining and Microscopy

For section immunofluorescence, organoids were isolated from Matrigel, fixed in 2% paraformaldehyde in 4°C overnight, washed, and embedded into paraffin blocks. Sections were cut and hydrated before staining. Sections were boiled with citrate (pH = 6.0), permeablilized in PBS supplemented with 0.2% Triton X-100 (PBST) and blocked with 2% normal donkey serum (Jackson ImmunoResearch) or Power Block Universal Blocking Reagent (BioGenex) for 1h at RT. Primary antibodies were then incubated at 4°C overnight. Subsequently, after wash with PBS, sections were incubated with secondary antibodies, stained with DAPI and then embedded using Vertashield (Vector labs). Images were captured on Sp8 confocal microscope (Leica) and processed using Photoshop CS4 or ImageJ software. Cell size of liver organoids were measured on organoid sections co-stained with membrane-labeling and DAPI by ImageJ software.

For Immunohistochemistry, after sections were made and hydrated, they were incubated with blocking buffer with H2O2 for 15 min and boiled with citrate (pH = 6.0). After cooling down, sections were treated with pre-blocking buffer and incubated with primary antibodies at 4°C overnight. Sections were incubated with secondary antibodies and DAB stained. Sections were enclosed with Pertex and images were taken on a DM4000 microscope (Leica).

For whole mount staining, organoids were harvested using cell recovery solution (Corning) and fixed in 4% paraformaldehyde at 4°C for 30 min. Organoids were then washed with PBT (PBS, 0.1% Tween), permeablilized in 0.5% PBST, blocked with 2% normal donkey serum in PBS or Power Block Universal Blocking Reagent (BioGenex) for 1h at RT and incubated overnight with primary antibodies. The next day, organoids were washed with PBT and incubated overnight at 4°C with secondary antibodies, Alexa Fluor-647 Phalloidin (both from Thermo Fischer Scientific) and DAPI (Invitrogen). Organoids were optically cleared in a glycerol-based clearing solution for 10 min prior to imaging. Organoid imaging was performed on Sp8 confocal microscope (Leica) or a Zeiss LSM 880 using a 25x oil immersion objective. Images were processed using Photoshop CS4 or ImageJ software and Imaris imaging software was used for 3D rendering of images.

Microarray

Total RNA was isolated from liver 3 days after 2/3 PHx and from undamaged liver. RNA was amplified, labeled and pooled for microarray analysis at the University of Hong Kong facility. Universal mouse reference RNA (Agilent) was differentially labeled and hybridized to the tissue. The data for the microarray analysis is deposited at Gene Expression Omnibus: GSE110292.

Flow cytometry (FACS)

For Albumin+ hepatocyte or Axin2+ hepatocyte sorting, hepatocytes were isolated by the two step collagenase perfusion method and stained with DAPI. Single live Tomato+ cells were sorted and collected into 15ml tubes or 384 wells plates for culture, mRNA or single-cell sequencing.

For ploidy sorting of hepatocytes, cells were stained with Hoechst 34580 (Invitrogen) at 37°C for 15 minutes and 2n, 4n, or 8n cells were separately collected as described before (Duncan et al., 2010).

Transmission EM

For Transmission EM, organoids were grown in Matrigel on 3 mm diameter and 200 microm depth standard flat carriers for high pressure freezing and immediately cryoimmobilized using a Leica EM high-pressure freezer (equivalent to the HPM10), and stored in liquid nitrogen until further use. They were freeze-substituted over 3 days at –90°C in anhydrous acetone containing 2% osmium tetroxide and 0.1% uranyl acetate at –90°C for 72 hours and warmed to room temperature, 5° per hour (EM AFS-2, Leica, Vienna, Austria). The samples were kept for 2h at 4°C and 2h more at room temperature. After several acetone rinses (4 × 15 min), samples were infiltrated with Epon resin for 2 days (3:1-3h; 2:2-3h; 3:1-overnight; pure resin-6h +overnight+6h+overnight+3h). Alternatively, chemical fixation with 1.6% glutaraldehyde was performed. The fixation was followed by dehydration in acetone and then embedding in Epon resin as explained. Ultrathin sections were observed in a Tecnai Spirit T12 Electron Microscope equipped with an Eagle CCD camera (Thermo Fisher Scientific, the Netherlands).

Functional Analysis of Hep-Orgs and Chol-Orgs

Hep-orgs of late passages were used for functional analysis. To access glycogen storage, we used periodic acid-Schiff (PAS, Sigma) staining. LDL uptake was detected with DiI-Ac-LDL (Biomedical Technologies). MDR1-mediated transport of rhodamine 123 was detected over a 10–15 minutes incubation. Mouse and Human albumin secretion was detected with Bethyl Elisa Kit and P450 activity was tested by Promega Kit. Human α1-Antitrypsin and human alpha-Fetoprotein (AFP) were detected by Elisa kit from Assaypro and R&D. All experiments were followed manufacturers' instructions.

Transplantation

Human Fetal-Orgs were used after differentiation in DM for 5–7 days on 2D collagen coated plates. Before transplantation, organoids were harvested and digested with trypsin digestion to produce single cells, filtered through at 70 μm cell strainer (BD Bioscience), washed and viable cell numbers were calculated by trypan blue exclusion. Hep-Orgs (Fetal-Orgs and PHH-Orgs) cells after digestion were maintained at 4°C in cold Hep-Medium until transplantation. 100,000 to 300,000 per mouse were injected intrasplenically into female FNRG mice preconditioned with one 70mg/kg dose of retrorsine, OSM, and $1x10^9$ genomic equivalents of an adenoviral vector expressing human HGF (Agilent). ALB and AFP levels were quantified by ELISA in blood serum obtained every 1–2 weeks after transplantation. Mice were sacrificed at various times (around 30 days and 90 days) after transplantation and liver sections were stained for human markers (hALB and NuMA).

QUANTIFICATION AND STATISTICAL ANALYSIS

Statistical Analysis

Data were compared between two groups of samples using the unpaired, two-tailed Student's t test. Error bar presented as mean+/− standard deviation or SEM and p value were calculated.

GSEA Analysis

Gene Set Enrichment Analysis (GSEA, Broad Institute) was used to classify different gene sets. Genes were ranked according to the expression level (upregulated or downregulated at least 5 folds) after partial hepatectomy. Then the bulk mRNA sequencing data of Hep-Orgs and Primary-Heps was submitted to GSEA list to pre-ranked modes

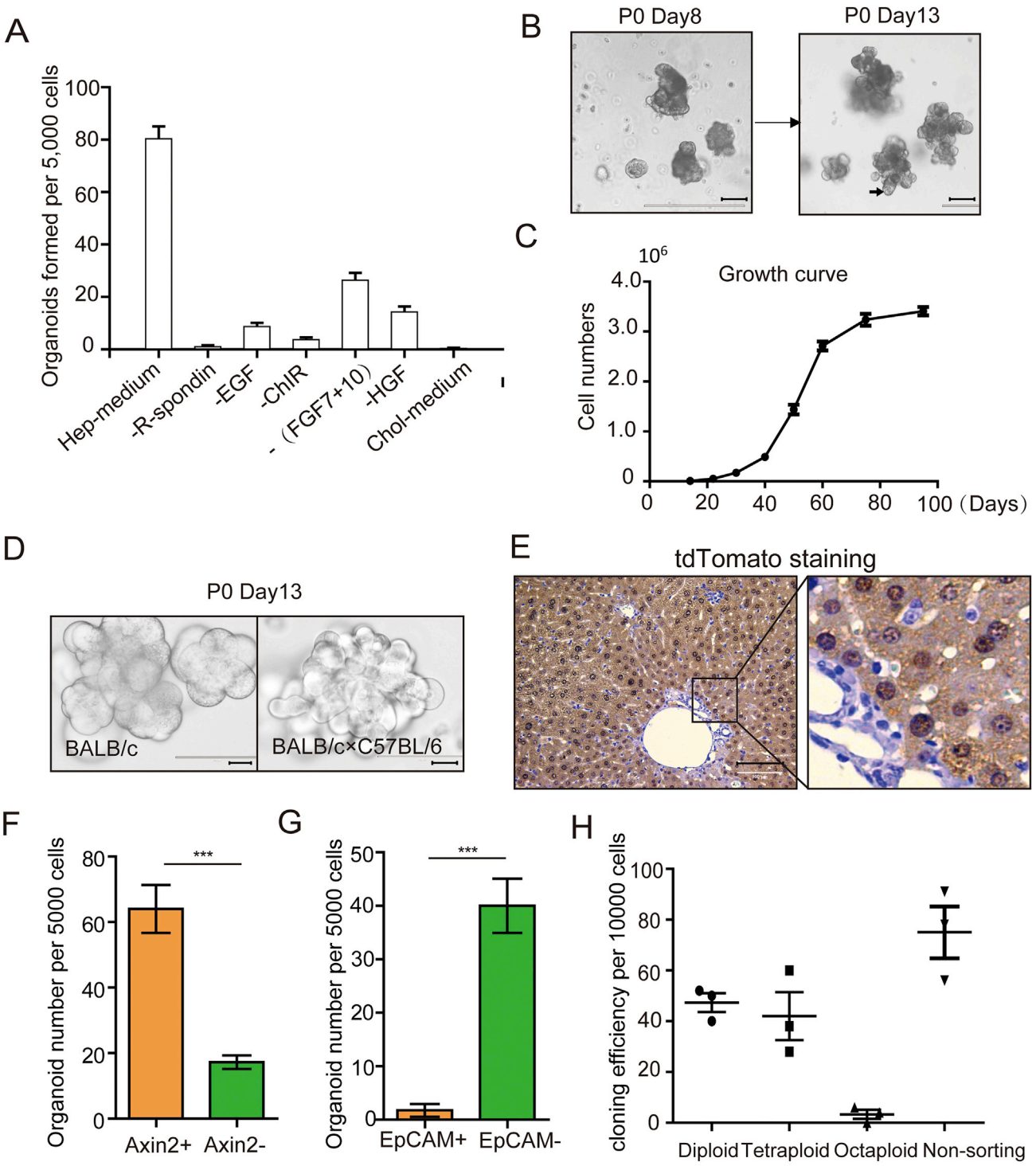

Figure S1. Hepatocyte Organoids Originate Mainly from Central Vein Hepatocytes, Related to Figure 1

(A) Numbers of Hep-Orgs per well in medium of indicated composition. Organoid numbers were counted on day 10 after seeding. Data are represented as mean SEM in triplicate wells.

(B) DIC images of Hep-Orgs growing in Hep-Medium at Passage 0 (p0) on day 8 and day 13 (the same field). Lipid droplet in organoids indicated with black arrow (black scale bar = 100 μm).

(C) Growth curve of Hep-Orgs (derived from primary mouse hepatocytes) followed from day 0 to day 100 after seeding. Please note leveling off during months 2–3. Data are represented as mean SEM for three adult male mice of the same age.

(legend continued on next page)

(D) DIC images of Hep-Orgs (derived from primary mouse hepatocytes of BALB/c mice or C57BL/6 x BALB/c F1 progeny) cultured in Hep-Medium analyzed at Day 14 (black scale bar = 25 μm).
(E) Immunohistochemical staining for tdTomato on mouse liver tissue section of *Albumin-CreERT2*; *Rosa26-LSL-tdTomato* mouse five days after a single dose of tamoxifen induction (black scale bar = 50 μm).
(F) Numbers of organoids formed per 5,000 cells FACS-sorted as Axin2 positive (Axin2+) or Axin2 negative (Axin2-). Experiments were performed in triplicate. Data are represented as mean ± SEM.
(G) Numbers of organoids formed per 5,000 Epcam+ cells. Experiments were performed in triplicate. Data are represented as mean ± SEM.
(H) Numbers of organoids formed per 10,000 cells (diploid, tetraploid, octaploid hepatocytes, FACS-sorted using Hoechst34580 and non-sorted hepatocytes). Data are represented as mean ± SEM.

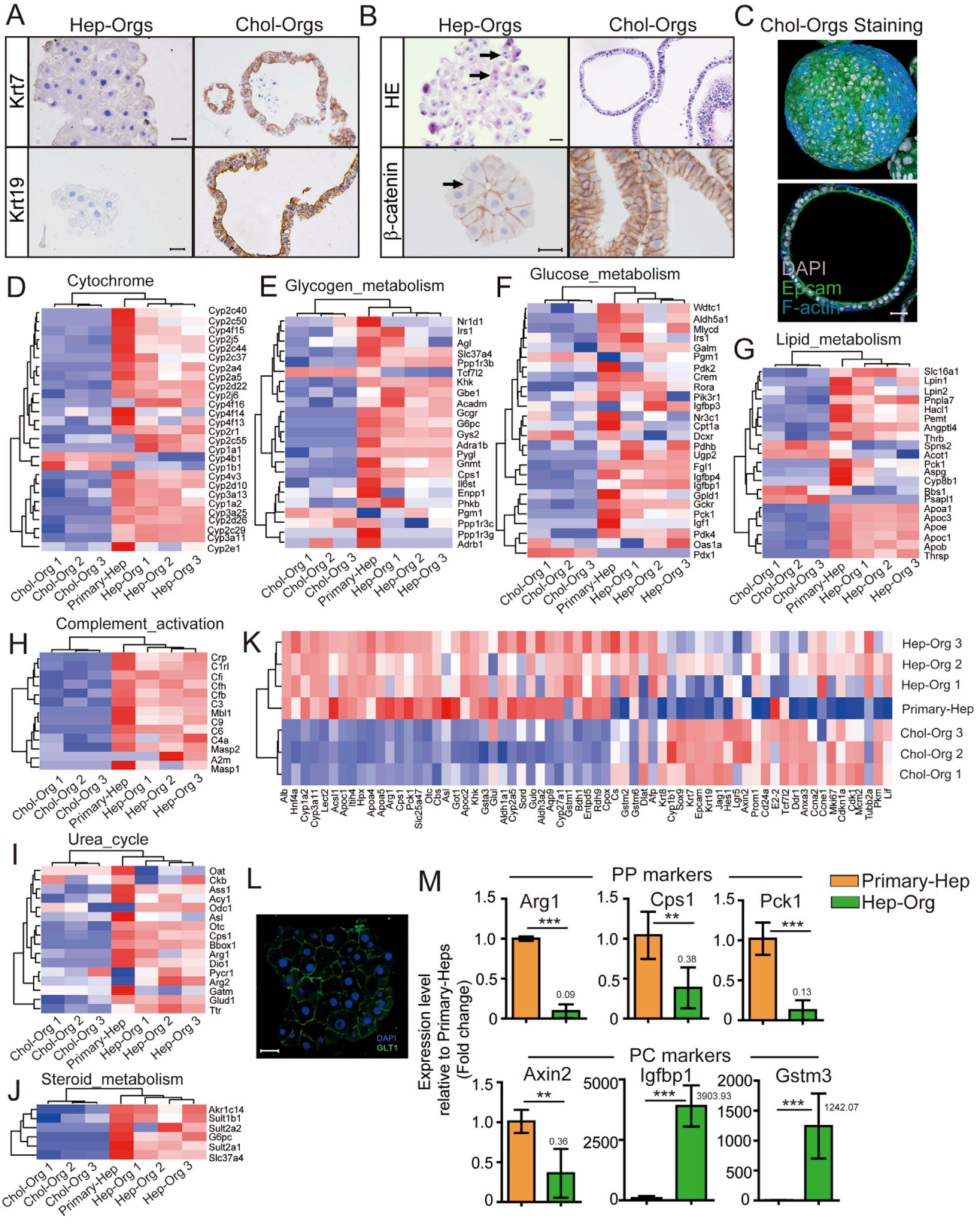

(legend on next page)

Figure S2. Comparison of Murine Hep-Orgs and Chol-Orgs, Related to Figure 2

(A) Immunohistochemical staining of biliary epithelial cell markers of Krt7 and Krt19 in Hep-Orgs and Chol-Orgs. Scale bar = 20 μm.

(B) Paraffin sections of Hep-Orgs and Chol-Orgs HE-stained (top) and stained for β-catenin (bottom). Arrows indicated binucleated cells in the Hep-Orgs (upper panel, scale bar = 20 μm. Bottom panel, scale bar = 25 μm).

(C) Confocal images of Chol-Orgs (z stack, top; single confocal section, bottom). F-actin (blue), Epcam (green), and DAPI (white). Scale bar = 20 μm.

(D–J) Heatmaps comparing Hep-Orgs (n = 3) with primary hepatocytes (n = 1) and Chol-Orgs (n = 3). Cytochrome activity (D), glycogen metabolism (E), glucose metabolism (F), lipid metabolism (G), complement activation (H), urea cycle (I), and steroid metabolism (J). Gene set was basically from figure S2 (Katsuda et al., 2017). Samples are the same as in Figure 2I.

(K) Heatmap of expression profile of liver genes comparing Hep-Orgs (n = 3), with Primary-Heps (n = 1), and Chol-Orgs (n = 3) with the full gene name list, used in Figure 2I.

(L) Immunofluorescence staining of Glt1 (green) and DAPI (blue) of a Hep-Org section. Scale bar = 20 μm.

(M) Comparison of pericentral (PC) and periportal (PP) marker expression in Hep-Orgs compared with primary hepatocytes. Data are represented as mean ± SEM. ** indicates $p < 0.01$, *** indicates $p < 0.001$.

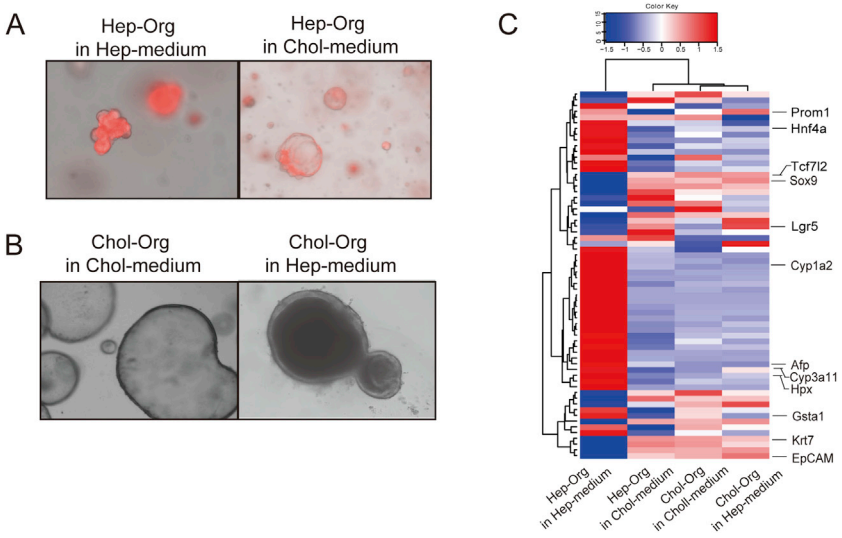

Figure S3. Hep-Orgs Transdifferentiate into Chol-Orgs in Chol-Org Medium, Related to Figure 3

(A) Fluorescent DIC images showing conversion of Tomato+ Hep-Orgs from Albumin-CreERT2; Rosa26-LSL-tdTomato into Chol-Orgs.

(B) DIC images showing typical change of Chol-Orgs in Hep-Medium.

(C) Heatmap of expression profile of RNA sequencing comparing Hep-Orgs with/without Chol-medium exposure and Chol-Orgs with/without Hep-Medium exposure for 10 days. Lane 1 and 3: Hep-Org 3 and Chol-Org 3 also appear in Figure 2I.

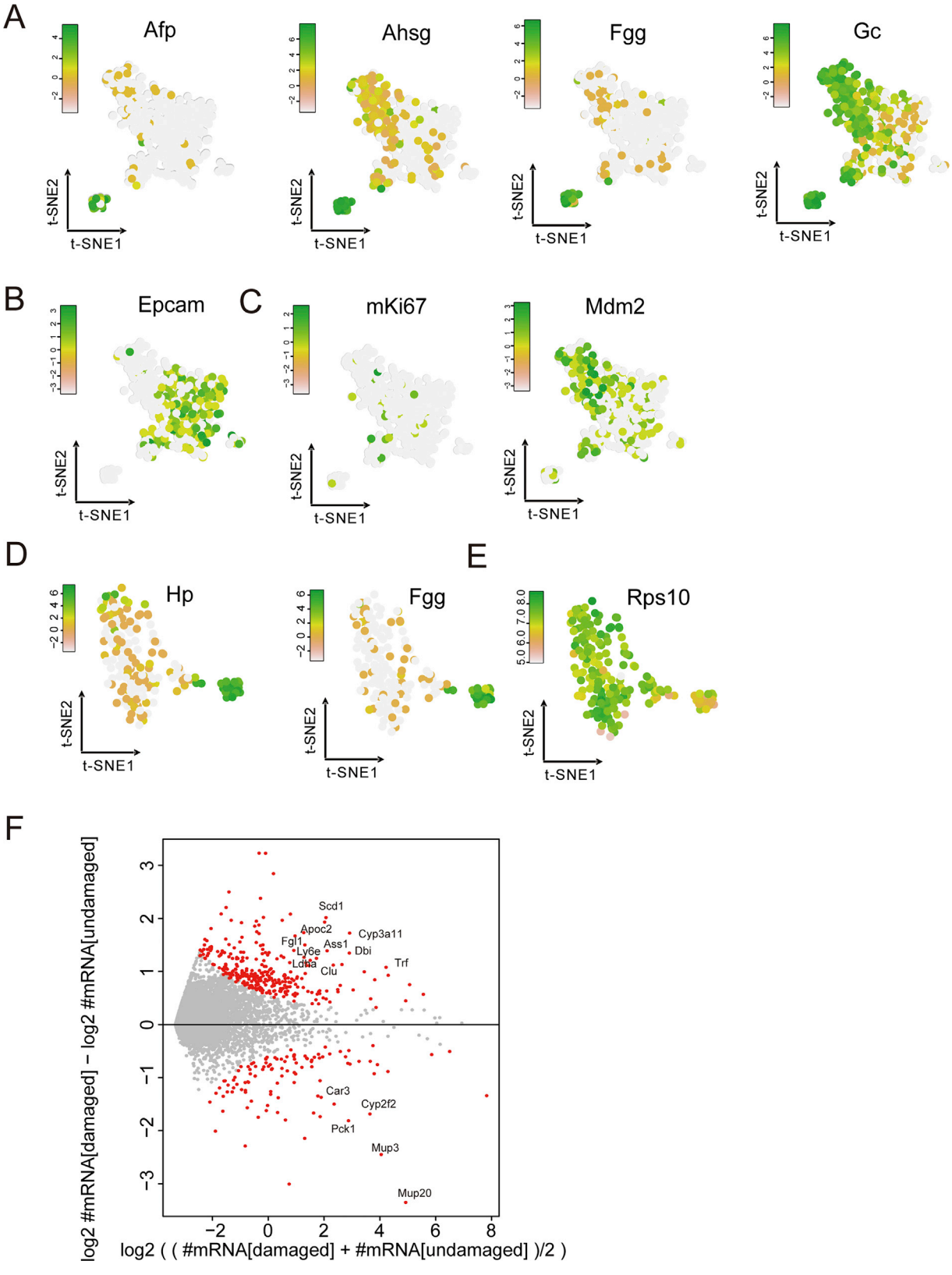

(legend on next page)

Figure S4. Gene Expression Analysis of Hep-Orgs and Chol-Orgs by Single-Cell Sequencing, Related to Figure 4

(A) t-SNE plot of cells color-coded for expression level of indicated Hepatic markers (Afp, Ahsg, Fgg and Gc) (B), Cholangiocyte marker (Epcam) (C), and cell cycle marker (mKi67 and Mdm2). Combined dataset of Hep-Orgs and Chol-Orgs. Expression is given as normalized log2 value.

(D and E) t-SNE plot of cells color-coded for expression level of hepatic marker (Hp and Fgg) (D), Cell cycle (Rps10) (E) in the Hep-Org dataset. Expression is given as normalized log2 value.

(F) Volcano plot showing genes differentially expressed between hepatocytes after PHx versus undamaged PHHs. Every dot represents a gene. Red dots highlight genes that show $\geq$2- or $\leq$2-fold change and a significance with p value < 0.05.

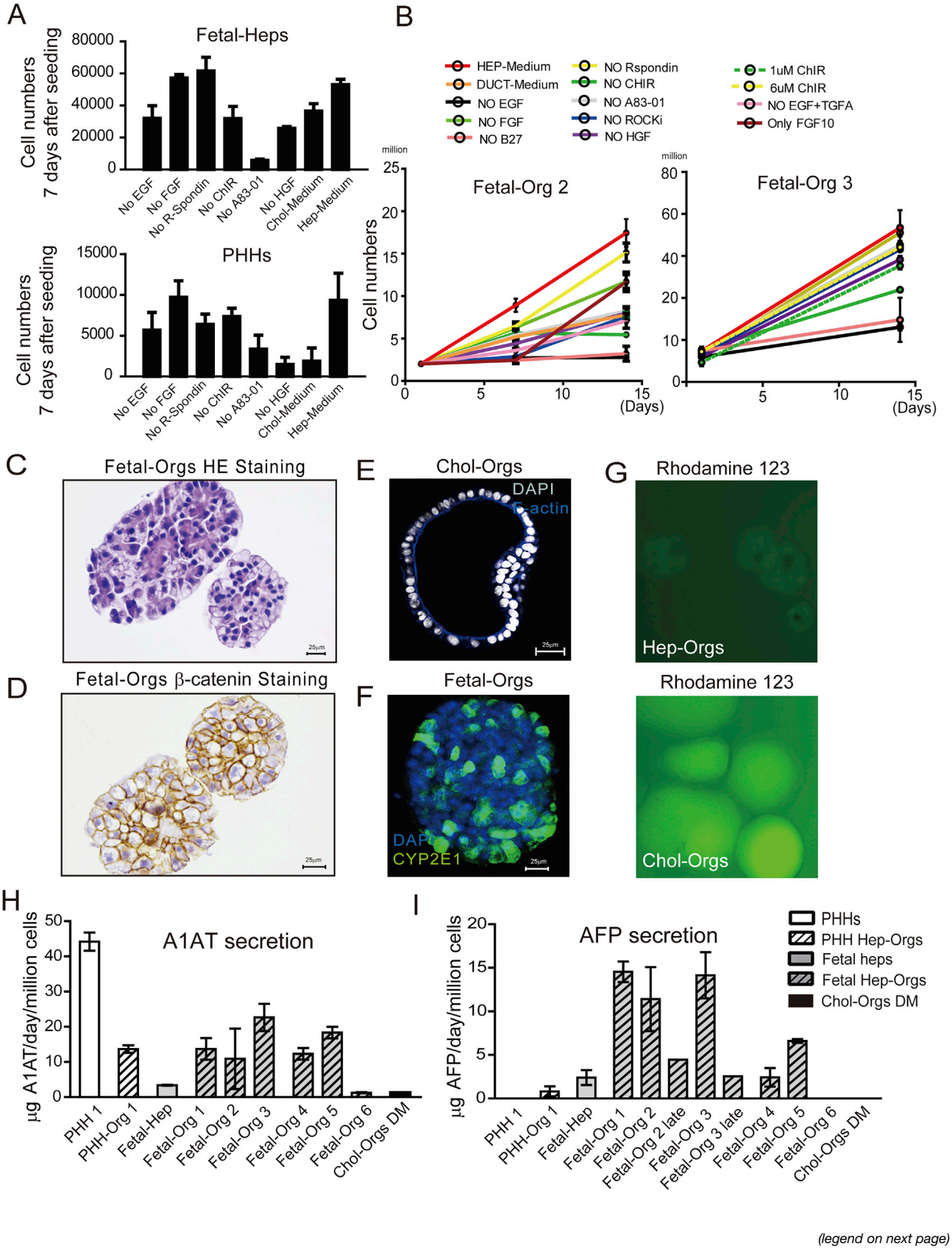

(legend on next page)

Figure S5. Establishment, Maintenance and Characterization of Human Hep-Orgs, Related to Figure 5

(A) Key components required for Hep-Org initiation from Fetal-Heps (top) or from PHHs (bottom). One of the main components (EGF, FGF, R-spondin CM, CHIR, A83-01, HGF) was withdrawn from Hep-Medium or Chol-medium was used to compare. Hepatocytes were cultured in different conditions. Data are represented as mean SEM.

(B) Key components for growth of two established Fetal-Orgs at P24, the coding corresponds to Figure 5J. One of the main components of Hep-Medium was withdrawn from Hep-Medium or Chol-medium was compared with Hep-Medium in Hep-Org growth maintain. Data are represented as mean SEM.

(C) PAS staining and (D) β-catenin (membrane labeling) of paraffin section of Fetal-Orgs cultured from human Fetal-Heps (scale bar = 25 μm).

(E) F-ACTIN Staining of human Chol-Orgs (single confocal plane).

(F) CYP2E1 Staining of Fetal-Orgs (single confocal plane).

(G) Representative image of uptake of rhodamine 123 dye in Chol-Orgs, but not Hep-Orgs.

(H) A1AT secretion measured in supernatant of cultured PHHs (white), PHH-Orgs (white striped), Fetal-Heps (grey), Fetal-Org (grey striped) and differentiated Chol-Orgs (black). Results are indicated as micrograms of albumin per day per million cells. Data are represented as mean ± SEM.

(I) AFP secretion measured in supernatant of cultured PHHs (white), PHH-Orgs (white striped), Fetal-Heps (grey), Fetal-Org (grey striped) and differentiated Chol-Orgs (black). "Late" is P22 from one well. All coding corresponds to Figure 5J and Figure S5H. Data are represented as mean ± SEM.

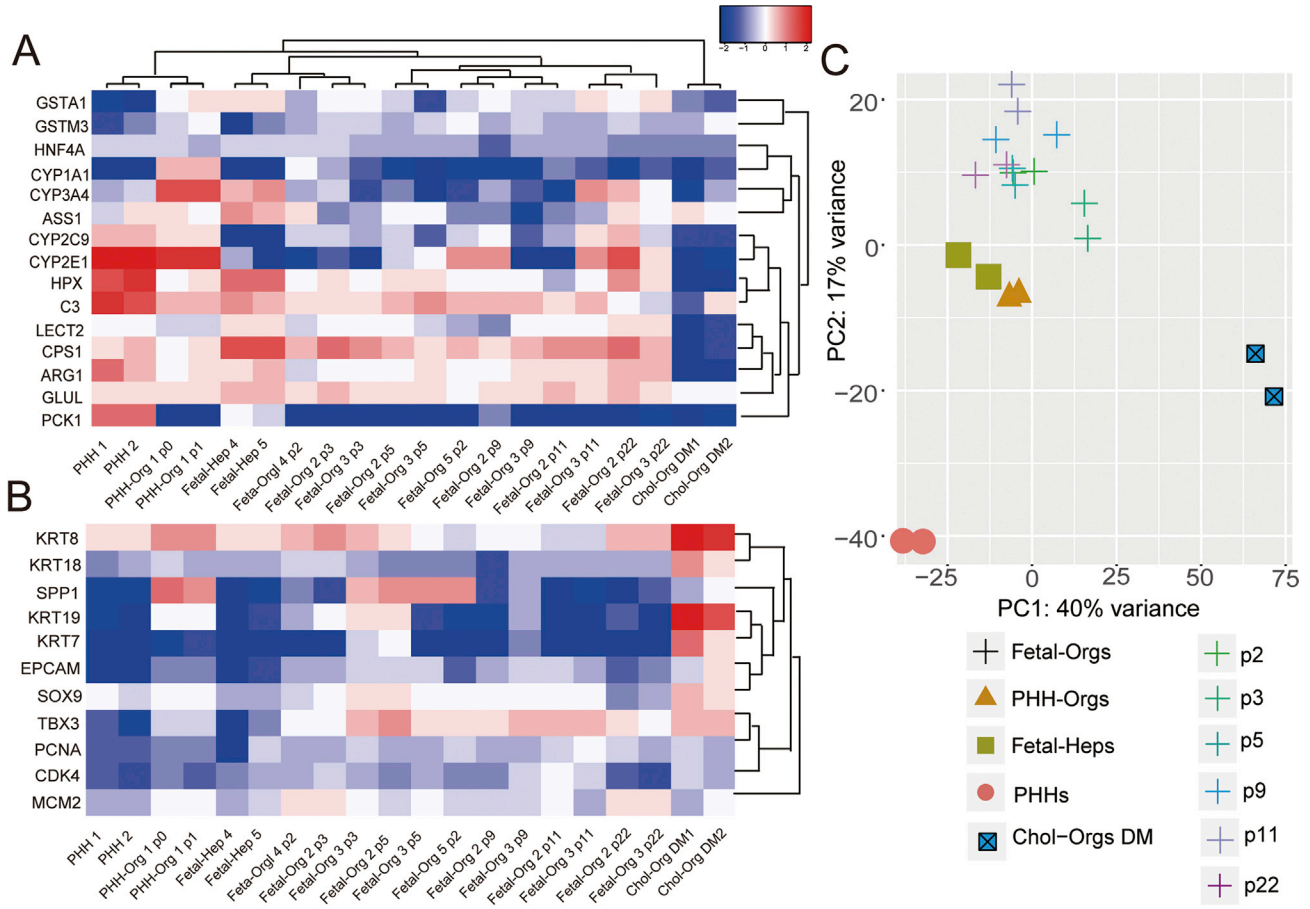

(legend on next page)

Figure S6. Transcriptional Comparison of Hep-Orgs, Chol-Orgs and PHHs, Related to Figure 6

(A) Heatmap of key hepatic gene expression in PHHs, PHH -Orgs, Fetal-Heps, Fetal-Orgs and differentiated Chol-Orgs.

(B) Heatmap of expression of progenitor, cholangiocyte and cell-cycle-related genes in PHHs, PHH -Orgs, Fetal-Heps, Fetal-Orgs and differentiated Chol-Orgs.

(C) Principal component analysis (PCA) analysis shows clustering of transcriptomic profiles of Hep-Orgs (PHH-Orgs and Fetal-Orgs) with human hepatocytes (PHHs and Fetal-Orgs).

(D–F) t-SNE plot of cells color coded for expression level for hepatocyte marker AFP, RBP4, APOA2 and MT1G (D), COL1A2 and FSTL1 (E), cell-cycle related genes PCNA and MKI67 (F). Expression is given as normalized log2 value.

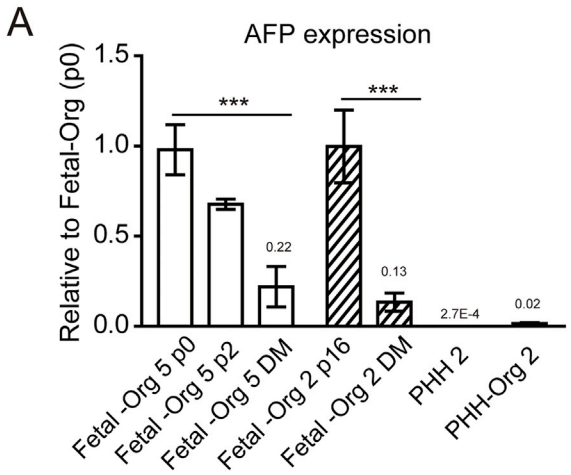

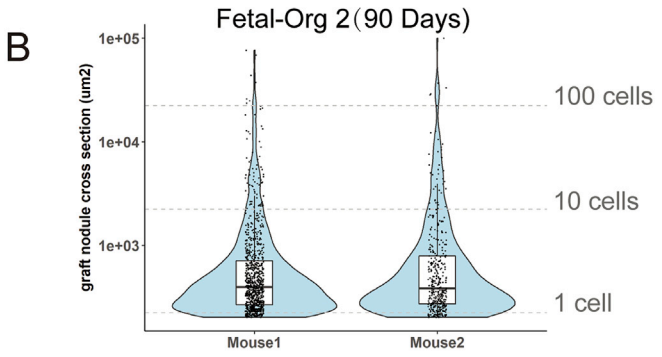

	Mouse 1	Mouse 2
Area analyzed(cm2)	1.93	2.65
Number of Nodules(>10)	76	40
Proliferative Nodule/cm2	39.34	15.08

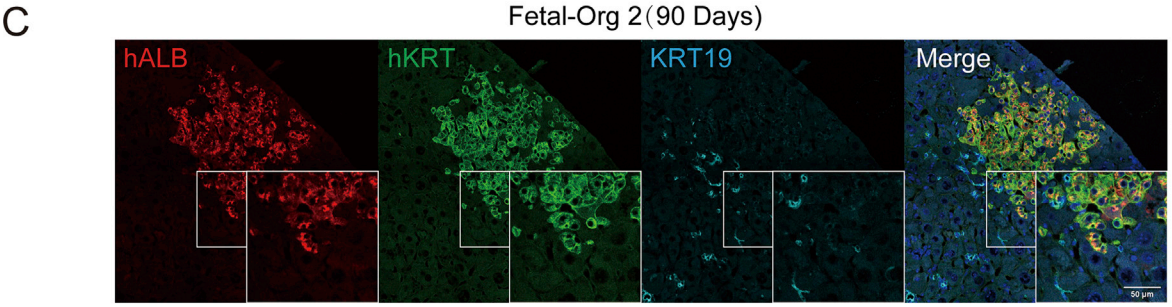

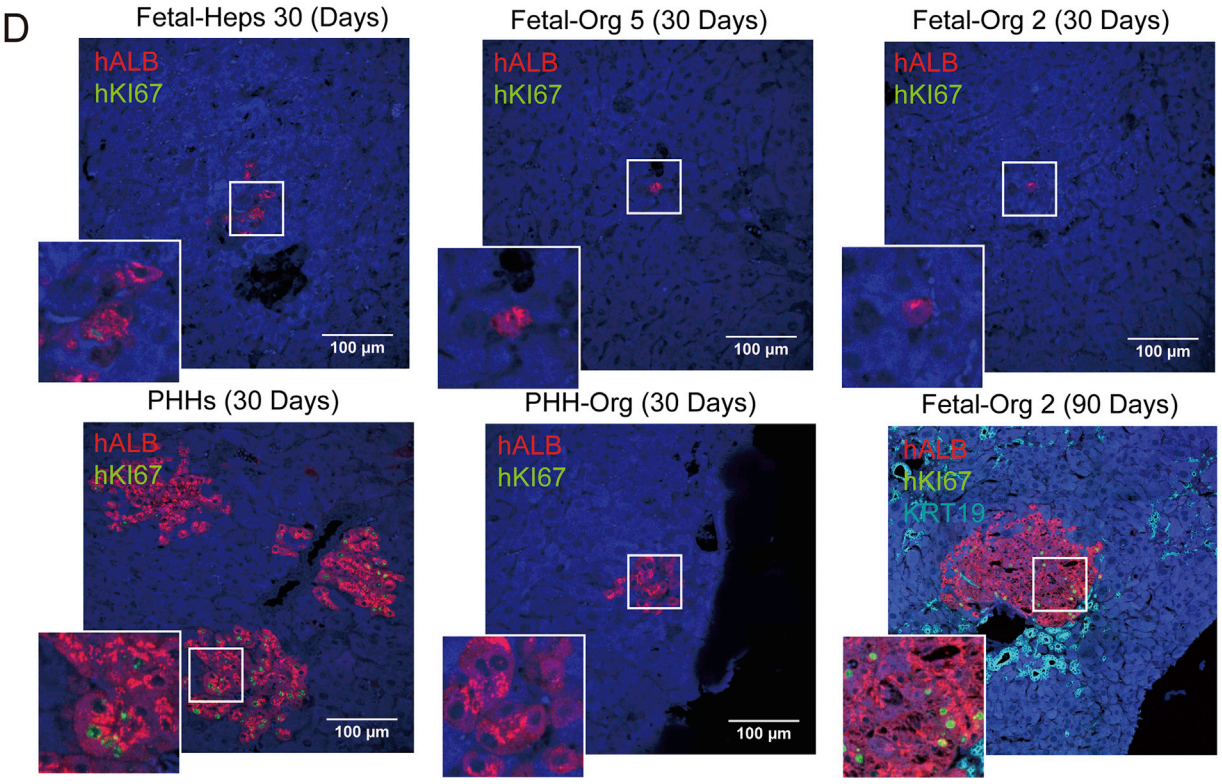

(legend on next page)

Figure S7. Engraftment and Repopulation by Human Hep-Orgs Compared with PHHs, Related to Figure 7

(A) AFP expression was reduced in differentiated Fetal-Orgs. Comparison was made between Fetal-Orgs of different passages, before or after differentiation with PHHs and PHH-Orgs.

(B) Graft nodule cross section quantified 90 days after transplantation of human Fetal-Orgs.

(C) Human ALB, hKRT, KRT19 and DAPI immunofluorescent staining of liver section of transplanted FNRG mouse 90 days after transplantation.

(D) Comparison of grafts 30 days after transplantation of PHHs, PHH-Orgs derived from the same donor, Fetal-Heps, and Fetal-Orgs (followed for 30 and 90 days) from the same donor.